APPLICATIONS OF URBAN MODELING USING VEGETATION-IMPERVIOUS SURFACE-SOIL AND LINEAR SPECTRAL MIXTURE ANALYSIS IN NON-WESTERN COUNTIES

by

Caleb Emir Gaw

A Thesis
Submitted to the
Graduate Faculty
of
George Mason University
in Partial Fulfillment of
The Requirements for the Degree
of
Master of Science
Geoinformatics and Geospatial Intelligence

Committee:

_______________ Dr. Anthony Stefanidis, Thesis Director

_______________ Dr. Anthony Stefanidis, Committee Member

_______________ Dr. Arie Croitoru, Committee Member

P. Agouris _______________ Dr. Peggy Agouris, Committee Member

P. Agouris _______________ Dr. Peggy Agouris, Department Chairperson

_______________ Dr. Timothy L. Born, Associate Dean for Student and Academic Affairs, College of Science

_______________ Dr. Vikas Chandhoke, Dean, College of Science

Date: 05/02/2013 _______________ Spring Semester 2013
George Mason University
Fairfax, VA

Applications of Urban Modeling Using Vegetation-Impervious Surface-Soil and Linear Spectral Mixture analysis in Non-Western Counties

A Thesis submitted in partial fulfillment of the requirements for the degree of Master of Science at George Mason University

By

Caleb Emir Gaw
Bachelor of Science
United States Air Force Academy, 2004

Director: Anthony Stefanidis, Associate Professor
Geography and GeoInformation Science

Spring Semester 2013
George Mason University
Fairfax, VA

ACKNOWLEDGEMENTS

I would like to acknowledge the fantastic support, guidance and council provided to me over the course of my studies by Dr. Anthony Stefanidis, Dr. Arie Croitoru, Dr. Kevin Curtin and Dr. Ron Resmini. Without their help, I would not be where I am today. I would also like to acknowledge the flexibility and understanding provided by Rachel Geyster at SAIC, who provided me the support to peruse my academic goals while working full time. Most importantly I would like to acknowledge the support and help provided by Dr. James Gaw and Khara Gaw; their constant support and willingness to look over my research was priceless.

TABLE OF CONTENTS

LIST OF TABLES

LIST OF FIGURES

LIST OF EQUATIONS

ABSTRACT

APPLICATIONS OF URBAN MODELING USING VEGETATION-IMPERVIOUS SURFACE-SOIL AND LINEAR SPECTRAL MIXTURE ANALYSIS IN NON-WESTERN COUNTRIES

Caleb Emir Gaw, MS

George Mason University, 2013

Thesis Director: Dr. Anthony Stefanidis

Developing accurate methodologies and models for using remotely sensed data is important in examining and understanding urban areas. Just as sensor types have evolved over time, the techniques and methods for modeling urban areas have been in constant development. In particular, there has been much development over the last 20 years increasing the efficiency and accuracy of the Vegetation – Impervious Surface – Soil (V-I-S) Urban model purposed by Ridd in 1995, through spectral mixture analysis. While many works have shown how to reduce errors within these processes and increase the accuracy of their results over their respective study areas, a fundamental question remains: are these models and techniques applicable to other urban areas outside of their study area? This work will address the logical development of the V-I-S urban model through spectral mixture analysis with the application to urban areas outside of western developed countries. The results will indicate that advances in spectral mixture analysis do increase the accuracy of depicting Vegetation, Impervious Surfaces and Soil, but that the V-I-S model does not accuracy accurately and consistently depict urban areas across the globe.

CHAPTER 1: INTRODUCTION

1.1: Overview

In 1995 M. K. Ridd from the center for Remote Sensing and Cartography and the University of Utah Research institute, Salt Lake City, Utah, published *Exploring a V-I-S (vegetation-impervious surface-soil) model for urban ecosystem analysis through remote sensing: comparative anatomy for cities.* Ridd proposed an ingenious new way of looking at urban classification, through the combined ratios of the three primary endmembers of vegetation, impervious surfaces and soil. Using these three components he went on to show how remote sensing, in particular satellite data, could be utilized over large urban areas in order to break down the area urban composition. Moving from areas of wilderness to high density residential and built-up urban areas to industrial sectors, Ridd showed how multiple cities could be described using the same model (Ridd 1995). Additionally, Ridd's model showed how an urban area could be described through temporal change as land-cover or land-use evolved from wilderness through the stages along the rural to urban continuum. Ridd's publication proved to be well-received, with 273 other works citing his work (Web of Science), and referencing his research for their applications with regards to urban classification. University text books such as the *Remote Sensing of Urban and Suburban Areas* site Ridd's model as being the framework for urban classification.

However, Ridd's model is just a framework. Since the 1995 publication, the GIS and Remote Sensing community has constantly sought to improve the methods and process for describing urban areas. Developments in technology have led to higher resolution satellite imagery as well as an increase in the amount of spectral variations captured in each pixel. At the same time, development in the processes for interpreting remotely sense data has greatly increased, moving from large scale classifications to pixel base classification into sub pixel classification. With better classification methods, others sought to increase the accuracy of the classification methods by developing procedures or process that would reduce the amount of error caused by the variations or geometrical inconsistencies within remotely sensed data. Over 18 years since Ridd's publication, the GIS and Remote Sensing communities' ability to analyze and describe urban and non-urban data from remote platforms has never been better.

1.2 Growing Trends for Modeling Urban Area

More important than the advancements in remote sensing and imagery processing are the numerous real life applications that analyses have derived from the available data. In particular, many works and projects have focused on ever increasing migration from rural setting to urban environments. With organizations such as the United Nations Population Fund (2007) pointing to the implications of the inward migration, in particular the ramifications for less developed nations, there has been a demand for developing better ways of analyzing, depicting and predicting urban growth. Bhatta et al. (2009) have shown how using remote sensing and urban classification can be used to depict the human impact on urbanization, in particular in studying the spatial statistics of impervious surfaces to show the rate and quality of growth in India. In China, where urbanization has been seen in the extreme, Li et al. (2003) and Lu and Weng (2006) have shown technics in using impervious surfaces to quantify and map out the hardest hit areas. Works, such as Almeidia et al (2005), have shown improvements in the techniques for classifying land-use changes within urban settings. With regards to disaster response, other, such as Alparslan et al. (2007) and Aydöner and Maktav (2009) have shown how remote sensing and urban classification can be used either as a model for disaster mitigation or as a method for facilitating urban resettling after a major disaster. These are just a small part of the total number of studies and publications that have been put forward to increase the GIS and Remote Sensing community's abilities to understand, depict and predict urban growth.

1.3 Motivation for Improving Ridd's Model

For all these models, there are always ways to improve individual components of the analysis and processing for urban model building. In almost all of these studies, the most prevalent components used in describing urban areas have been elements such as impervious surfaces or land-use via vegetation analysis such as the normalized difference vegetation index (NDVI). However, the models that use a single element to describe very complex and divers settings often seem lacking even if very informative in their own right. One example is that of the earlier mentioned work by Bhatta et al (2009) which studied the degree-of-freedom, degree-of-sprawl and degree-of-goodness using impervious surfaces. While very descriptive of the urban growth rate, it could not differentiate between the different components that made up the urban setting; thus their analysis was limited to the growth of “urban or non-urban.” Looking back to the 1995 V-I-S model that broke down the urban setting into clusters of possible classifications along the continuum of three primary components, it would be extremely powerful to be able take the same spatial statistical studies from Bhatta et al. (2009) and apply them to the same area across a variety of different urban classifications. Instead of the rate and quality of growth of “urban vs. non-urban,” it would be far more telling to show the rate and quality of growth for low residential, compared to high residential, compared to industrial, compared to the central business district (CBD) and so on. The same argument could be made for multiple other situations, from disaster mitigation to urban planning using historical contexts.

1.4: Primary Research Question, Methods and Data

Before the Ridd’s model can be directly used across these different studies, the basic question must be asked: is Ridd’s 1995 V-I-S model for urban classification applicable to areas outside that from which it was derived? In addition to this question, is the question: how should Ridd’s 1995 V-I-S model be applied using remotely sensed data? While many works have directly sought to answer the question regarding the applicability of Ridd’s V-I-S model (Ward et al. 2000; Phinn et al. 2002; Wu and Murray 2003 and Wu 2004), they have all always focused on the same basic urban environment: well established urban areas within developed countries.

This work’s primary focus is to establish the degree in which Ridd’s (1995) V-I-S model can be applied to urban areas outside of developed counties. In answering this question, this work will use current methods for sub pixel analysis using a normalized spectral mixture analysis purposed by Wu (2004) to three areas outside of the standard cities from developed counties. In particular, this work will look at the usability of Ridd’s (1995) V-I-S model and Wu’s (2004) normalized spectral mixture analysis over the areas Coban, Guatemala, İzmit, Turkey and Semey, Kazakhstan, in addition to the same city of Columbus, Ohio that was used in developing Wu’s (2004) methodology as a control.

In addition, this work will use Landsat ETM+ and TM imagery as the primary data source for performing the spectral mixture analysis and analysis of Ridd’s (1995) V-I-S model. While current sensors are able to provide a much higher resolution than the Landsat ETM+ and TM 30 meter resolution, as well as more available bands, the Landsat program has one of the world’s largest and longest collections of imagery across the globe. While using current sensors would produce more accurate results, the use of Landsat allows researchers to complete more in-depth temporal studies of urban areas and provides more directly available cost effective data.

1.5 Summary

In order to answer the question of applicability of Ridd’s V-I-S urban model, this work will review the literature surrounding the basic questions of how to define urban areas, the development of Ridd’s model and the progress made to improve the implementation of his model. Additionally, this work will review the literature regarding the use of spectral mixture analysis for implementing Ridd’s model and the proposed methods of normalizing the spectral mixture analysis. Using the methodologies described throughout the literature review, this work will show how to apply the procedures to Landsat datasets over various urban areas. The work will then review the accuracy of results as they pertain to estimation of impervious surfaces as well as their correlation to categories of urban development within Ridd's model.

In conclusion, while this work will show how the use of Ridd's (1995) model has been widely accepted and used in multiple studies, the improvements in processing remotely sensed data, and the appropriate use and application of Wu's (2004) normalized spectral mixture analysis, the results will also show the limited application of Ridd's (1995) model as it was originally developed. In particular, this work will show that while Wu's (2009) normalized spectral mixture analysis can successfully extract urban components along the V-I-S model, they fail to fall within the well described setting of Ridd's (1995) model. This work will show that, while an excellent starting point for urban analysis, in its original form Ridd's (1995) model is not applicable to areas outside of well established, developed nations. Instead of closing the door, this work will suggest that its conclusions provide an initial logical process for the analysis of distinct and very different urban environments. Instead of concluding an end to the quest to build a more efficient and affective urban model, this work will argue that Ridd's (1995) is just the very beginning and that there is much upon which we can improve.

CHAPTER 2: LITERATURE REVIEW

2.1: Defining Urban Areas for Remote Sensing

The core of this work addresses the methodologies and processes used to model urban environments correctly and accurately through remote sensing. Yet, before the specific methods and process used be appropriately described, the very most basic question must be addressed: “How does one define an urban area?” John R. Weeks begins the process of answering this question in Chapter 3 of *Defining Urban Areas*, in “Remote Sensing of Urban and Suburban Areas” by quickly showing the difficulties therein. Weeks argues (for the purpose of remote sensing) that “Urban” is a characteristics of place as opposed to people (Weeks 2010: p 33)—the question is better answered in terms of the physical components of the areas instead of the individual, population or societal components of the same physical area. Nevertheless, Weeks acknowledges that concept of “Urban,” as a function of area, is still a very complex subject and can be described in complex terms as functions of: (1) sheer population size, (2) space (land area), (3) ratio of population to space (density or concentration), and (4) economic and social organization (Weeks 2010: p 34).

In order to place the importance of how to define Urban Areas, Weeks points to the statistics from the United Nations Population Division (2008) that by the middle of the 21st Century almost two of every three people worldwide will reside within an urban environment (Weeks 2010: p 34). More strikingly are the statistics that in 1850 only 2%

of the world population lived in urban areas, yet within only a hundred years the number had jumped to 16%. In half the same time, by 2000, the world urban population was at 50% (Weeks 2010: p 34). This staggering mass movement of people from rural settings to urban setting has become a defining characteristic of the modern world, which emphasizes the importance of being able to define the "urban" characteristics.

Within the context of the UN statistics, Weeks discusses the urban transition from Rural to Urban over the last 200 years by referencing the technological advancements that allowed the possibility of large cities to exist as well as the technological advancements that helped encourage the urban migration (Weeks 2010: p 35). These technological advancements were not only important for allowing cities to accept larger population densities, but also provided the mechanization of agricultural areas to allow for smaller rural populations to support the food needs of the growing urban areas (Weeks 2010: pp 35-36). Expanding upon the move from rural to urban areas, Weeks argues that Rural to Urban should be explored as a continuum as opposed to a dichotomy (Weeks 2010: pp 36-38) and begins arguments for using Remotely-Sensed data to measure indirectly the spectrum of rural to urban settings (Weeks 2010: pp 38-39). While Weeks references his earlier argument (Weeks et al. 2005) that census and survey data should be used for developing the urban-rural index, for the purpose of remote sensing, the focus here is to define the methodologies and development of the "individual picture element (pixel)" as the primary method for describing the Urban-Rural areas (Weeks 2010: p 39). To this point, Weeks references the model developed by Ridd (1995) of Vegetation – Impervious Surface – Soil (V-I-S) as a guide for using spectral mixture analysis (SMA) to characterize the individual picture element (pixel) off the Urban-Rural continuum (Weeks 2010: p 40). Furthermore, Weeks shows how several different studies from Brisbane, Australia (Phinn et al. 2002) to Columbus, Ohio (Wu and Murray 2003) have successfully employed Ridd's (1995) V-I-S model to depict the Urban-Rural characteristics (Weeks 2010: p 40). In summary, Weeks argues that Ridd's (1995) V-I-S can be used in a schematic way to show the movement from Wilderness, through rural areas, to Urban Cities, seen in Figure 1 (Weeks 2010: pp 40-42). In this figure Weeks argues that Rural to Urban is not binary, but is a continuum with the types of spectral signature changing with the change in the level of urban development.

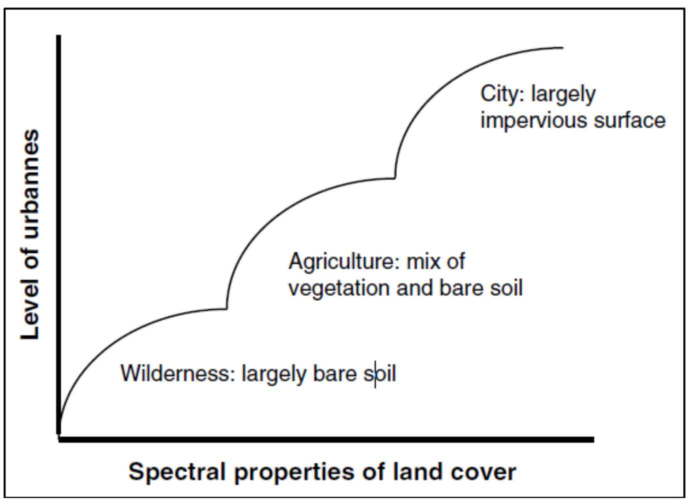

Figure 1: Land Cover vs. Urbanization. Here the X-axes is not depicting a specific change in wavelength, but that the spectral properties change as they move from non-Urban to Urban environment. To this point, Weeks notes that the "Urban gradient may be discontinuous." (Weeks 2010: p 41)

Although Ridd's (1995) V-I-S model for classifying urban areas is the primary focus of this work, it is important to note that the individual components (vegetation, impervious surfaces and soil) have all been used in different degrees to classify Rural-

Urban settings or model urban growth. Most common is the use of impervious surfaces as a classifier of urban areas (often referred to as “built-up” areas). Sudhira et al. (2004) use impervious surfaces (referenced as “urban build-up”) in their modeling of urban sprawl in India. In their methodology, Sudhira et al. (2004) use impervious surfaces derived from multi spectral LISS satellite imagery in conjunction with Survey of India toposheets to distinguish the extent of urban built-up areas and modeled the urban sprawl across a 30 year period in conjunction with population data reported by the Census of India (Sudhira et al. 2004). Other, more recent studies have also used impervious surfaces to detect urban sprawl using special statistical analysis. Bhatta et al. (2010) extracted impervious surface pixels from Landsat TM and MM as well as IRS LISS over a 30 years period and quantified the change through the degree-of-freedom (Pearson’s chi-squared statistics,) the degree-of-sprawl (Shannon’s entropy statistics) and the degree-of-goodness (statistically comparing the observed growth and expected growth with the magnitude of compactness or infilling). In essence, Bhatta et al. (2010) were able to classify the “quality” of urban growth through the change of impervious surfaces to locate planed growth and unplanned growth as well as helping to identify sustainable growth and non-sustainable growth.

2.2: Ridd’s V-I-S Urban Model

As documented by Weeks as well as numerous other authors also mentioned in this work, Ridd’s 1995 *Exploring a V-I-S (vegetation-impervious surface-soil) model for urban ecosystem analysis through remote sensing: comparative anatomy for cities* provides a fundamental standard model for describing the composition of urban environments. Like many authors, Ridd was answering what he described as the call for "standards in parameterizing biophysical comparison of urban environments" (Ridd 1995). Ridd argued that remotely sensed data, in particular the pixel, could be used as the "fundamental building block towards objective and quantitative characterization of urban morphology" (Ridd 1995: p 2116). In his work, Ridd acknowledges the previous work done to describe urban areas using the "positive relationship" between red and near-infrared wavelengths (captured using remotely sensed imagery) that help distinguish what Ridd references as the "soil line" or "non-vegetation line" in urban areas—whereas the definition of urban or human settlement is more binary (urban or non-urban / vegetation or non-vegetation). Ridd however, argues the need to expand the mechanisms for characterizing in more diversity the characteristics of the urban area (Ridd 1995: p 2116).

In this, Ridd starts by ignoring water surfaces and instead focuses on the combinations of impervious surfaces, green vegetation and exposed soil, as being "the most fundamental components of the urban ecosystem, in terms of contrasts with the surrounding environments as well as contrasts within the city" (Ridd 1995: p 2166). In essence, Ridd (1995) argues that the fundamental building blocks needed to describe the Urban-Rural areas can be broken down to the composition of the components Vegetation (V), Impervious surfaces (I) and Soil (S) at a pixel level. Most importantly, as opposed to binary approach, Ridd (1995) argues that a V-I-S Urban-Rural modeling can be described as the continuum between the three main components allowing for a much larger degree of flexibility in describing the different Urban-Rural components. In order to demonstrate this model, Ridd (1995) used a sampling frame of one central city block over Salt Lake City, wherein he sampled discrete point from high quality CIR photography at 1:30,000 scale data and recorded their results as to whether the individual point was composed of vegetation, impervious surfaces, or soil. From these results across all the sampling frames, Ridd tabulate natural breaks within the V-I-S variation as they applied to the characters of the urban area.

In order to tabulate these results, Ridd employed the use of triangular coordinates, which is used to depict how three-component blends can be used graphically to represent the overall mixture as well as the variations therein. As described by Yates (1996), triangular coordinates are well used across disciplines, such as physical chemistry and geology, and even for non-scientific studies such as pottery, which uses triangular graphs to show how three glazes can be blended to produce variations for a finished product. The tabulation of the triangular graphs rely on properties of the equilateral triangle (formulas for deriving area and simple trigonometric functions) and plotting the individual components ratios between the three endmembers within the triangle.

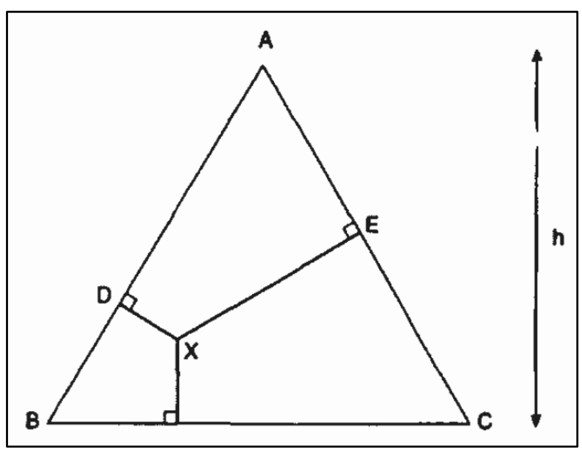

Figure 2, the basic model for the theory of triangular coordinates
According to Yates, the premise of triangular graphs "relies upon the fact that for any point *X* within an equilateral triangular ABC (see Figure 2) the perpendicular distance to each side (DX, EX and FX) add up to the perpendicular height of the triangle *h."* (Yates 1996: p 23)

Over several zones within Salt Lake City, Ridd found that common ratios of V-I-S could be used to successfully depict corresponding elements of the urban environment (See Fig. 4) (Ridd 1995).

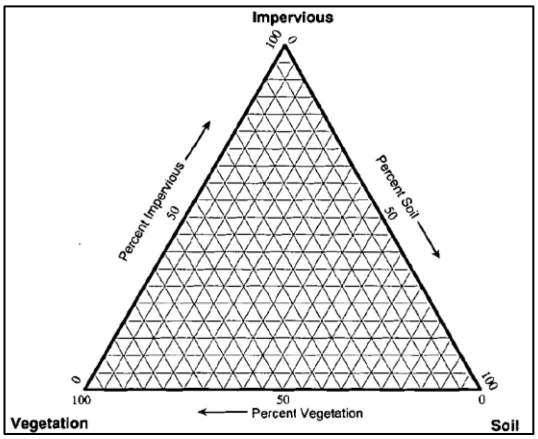

Figure 3 Ridd's VIS by % breakdown
(Ridd 1995 P. 2169)

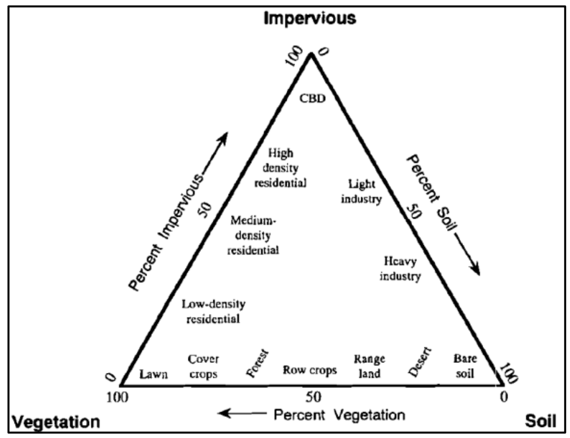

Figure 4 Ridd's VIS Urban Model
(Ridd 1995 P. 2173)

In particular, Ridd found that traditional land use from low density human residence through high density human residence, up to the central business district, could be best described through the ratio of green vegetation and impervious surfaces. Industrial land use, on the other hand, followed more strongly along the ratio of soil and impervious surfaces. Ridd found that the ratio of soil and vegetation could be best used to depict the change from natural land cover, such as deserts and forests, to human influenced land use such as residential lawns and agricultural (Ridd 1995).

In addition to being able to describe the urban environment by comparing the interaction of these three core aspects, Ridd (1995) also argues that modeling using V-I-S could also provide valuable temporal information through the study of change in an area's environmental ratios of V-I-S, along the line of moving from rural to urban (Ridd

1995). In the figures below, Ridd suggested in his conclusion that future studies of urban areas using the V-I-S model over a period of time could be used to anticipate changes in the urban environment.

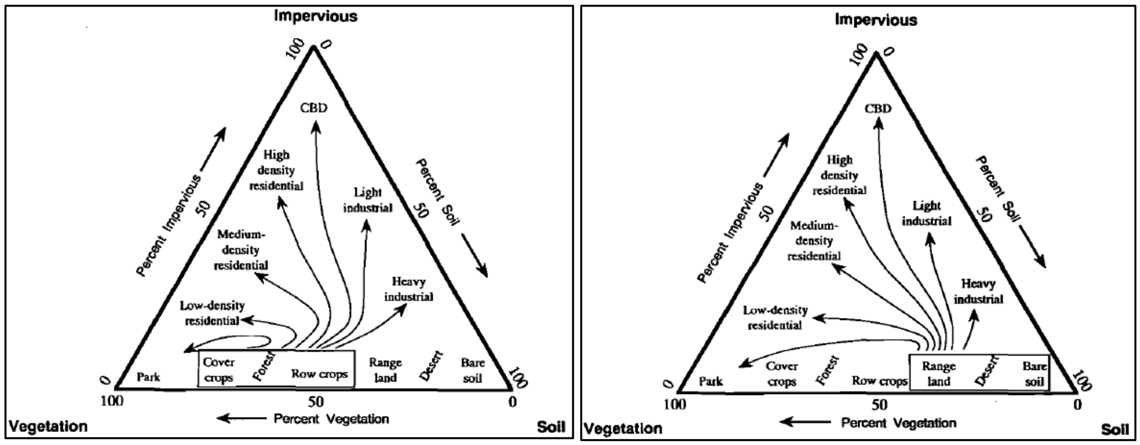

(A) (B)

Figure 5 Ridd's model anticipating changes along the V-I-S continuum. (A) "Where green landscape becomes urbanized"; (B) "Where dry landscapes become urbanized."
(Ridd 1995: p 2182)

Regarding the question of pixel size for best implementing the V-I-S model, Ridd (1995) acknowledged the limited spatial and spectral resolution of satellite data at the time of his publication. In particular, Ridd mentions the introduction of the Landsat system in 1972 with the Multispectral Scanner System (MSS) with a 79-m spatial resolution. While the MSS was able to provide an assortment of land-use or land-cover categories, Ridd (1995) argued that at a resolution of 79-m, there was often an "unclear distinction between the two" (Ridd 1995: p 2174), with Ridd pointing to the work by Foster (1983, 1985) supersizing the problems of trying to classify mixed pixels at this resolution. Instead, Ridd (1995) points to the "Thematic Mapper (TM) with its 30-m spatial resolution and seven spectral bands which makes it possible to identify several discrete urban surface covers" (Ridd 1995: p 2174). Ridd references studies over Toronto

(Gong and Howarth 1990) and the United States (Welch 1983) using 30-m resolution to successfully map urban areas, while other locations, such as China (Welch 1982) may require 10-m resolution to for accurate mapping of urban features. Regardless, Ridd acknowledges that better spatial resolution will always be beneficial (Ridd 1995: p 2174), but with the wide availability of 30-m Landsat TM data over a long period of time Ridd's V-I-S model opens a great multitude of areas across the globe to study.

2.3: Implementing Ridd's Model in Ward et al.

Evolving the fundamental V-I-S model proposed by Ridd (1995), Ward et al. (2000) developed a method of classifying urban areas at a per pixel level using Landsat TM imagery in *Monitoring Growth in Rapidly Urbanizing Areas Using Remotely Sensed Data*. Using Landsat TM's imagery over the Gold Coast in southeast Queensland, Australia, Ward et al. (2000) utilized the normalized difference vegetation index (NDVI) to produce unsupervised classification of their Area of Interest (AOI). Additional unsupervised classifications were then applied to the NDVI vegetation classified segments to better separate vegetation components as well as unsupervised classifications to the Soil-Impervious Surfaces Classes (See Figure 6).

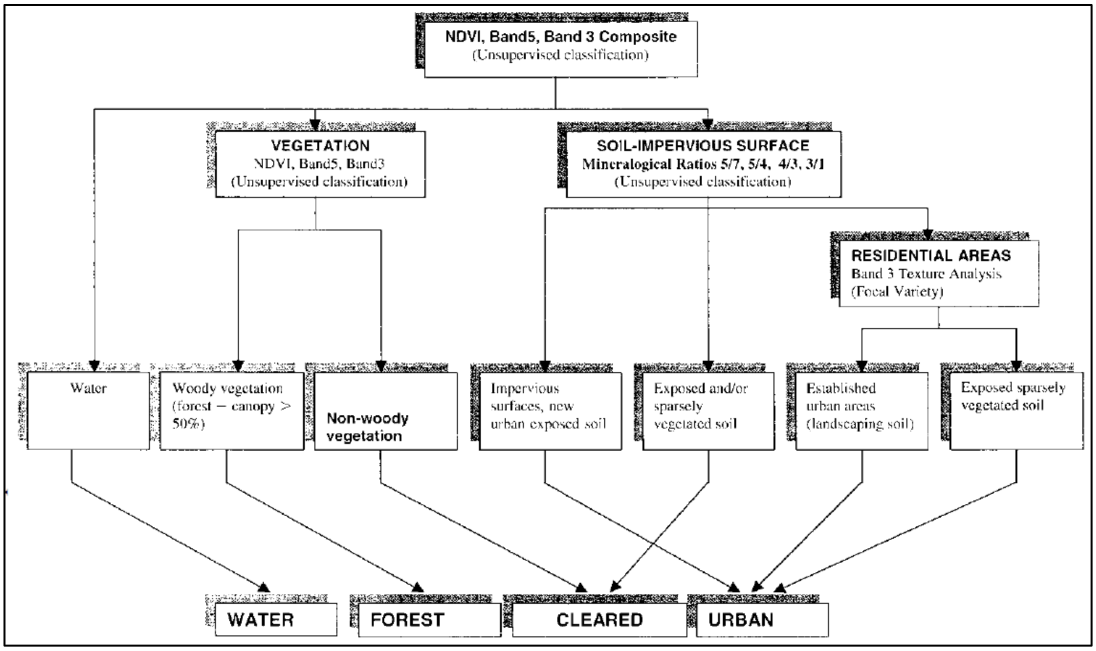

Figure 6 Ward et al.'s methods for classifying urban areas (Ward et al. 2000 p 376)

While not remaining true to the continuums along the V-I-S spectrum of Ridd's (1995) model, Ward et al. (2000) was able to create an overall 4-Endmember classification of Water, Forest (Ridd's 'green' vegetation), Cleared (Ridd's soil or exposed earth) and Urban, without any further subdivisions. With regards to these classifications, Ward et al. (2000) identified a fundamental problem with their methodology: exposed soil can belong to both the Urban and the Cleared class. Comparing their results against true color aerial photos at a 1:5,000 scale, the work found an overall adjusted classification accuracy of 83%, although their 'Cleared' class proved to be the most inaccurate with most commission and omission errors occurring with the 'Urban' class. Although problematic, the same model was applied to a temporal study over the same AOI to depict the percent change in urban area over a seven year period. In their study, Ward et al. (2000) reported accuracy of simulated urban growth to actual urban growth at being a “reasonable” 63%, with the majority of the errors due to an over-estimation of in-filling within original urban areas--showing faster than actual growth (Ward et al. 2000: p 383). While problematic in classifying Urban and Cleared area, the work was able to demonstrate that it was possible to use a modified version of Ridd’s V-I-S model to depict urban areas as well as urban growth.

2.4: Use of Spectral Mixture Analysis in Phinn et al. (2002)

While Ward et al. (2000) demonstrated an application of Ridd’s (1995) V-I-S model and identified problematic areas therein; other works covered the issues of per pixel classification with regards to same study of urban modeling. Phinn et al. (2002) address the issues of pixel level classification mentioned earlier regarding and specific to remote sensing platforms with > 20-m spatial resolution (L-resolution. They discussed five recurrent research themes:

1: Delimitation of land-cover and land-use types (Gong and Howarth 1992)

2: Assessment of the utility of texture measures to aid in separating urban land-cover and land-use types (Gong and Howarth 1990, 1992)

3: Mapping areas of impervious and pervious surface for input into energy and moisture flux models (Gong 1993)

4: Mapping Land-cover and land-use change in urban areas (Gong 1993)

5: Application of empirical models to estimate biophysical, demographic and social variables (Forster 1983, 1993. Jensen et al. 1994, Lo 1997, Lo and Faber 1997)

Simply put: “Per-Pixel classifications do not produce accurate results for urban land-cover mapping in L-resolution scenes” (Phinn et al. 2002: p 4132). To address these issues while using L-resolution data, Phinn et al. propose using spectral mixture analysis (SMA) to estimate the percentage of the urban composition within each pixel—moving the classification method of Ridd’s (1995) V-I-S from per-pixel to sub-pixel (Phinn et al. 2002: p 4133). Instead of creating a classification method where each pixel has a single signature across the available bands, SMA will extract the different components that make up the pixel’s overall signature based upon specific endmembers (primary components) defined prior to applying SMA (i.e. pixel X has a signature Y, but using SMA one can derive the percent signature A, B and C for the same pixel). Using Landsat TM and high resolution aerial imagery over Brisbane, Australia, Phinn et al. (2002) used spectral unmixing and direct interpretation to develop an “operational” method of implementing the V-I-S model.

To demonstrate their move from per pixel to sub pixel classification, Phinn et al. (2002) conducted three separate VIS classifications: (1) per pixel image classification using a hybrid approach from Ward et al. (2000) using a Normalized Difference Vegetation Index (NDVI), (2) a VIS classification extracted from aerial photography, and (3) a constrained spectral unmixing to match Ridd’s V-I-S requirements using the established SMA procedures for multispectral data from Wessman et al. (1997), and Metternicht and Fermon (1998). With regard to the per pixel classification, Phinn et al. (2002) found that separating impervious surface areas from soil areas was problematic for classification, although classifying water and vegetation proved much clearer. However, the High/Low-Density urban ratio between Vegetation and Impervious surfaces (from

Ridd's V-I-S model) did not provide any natural groupings, nor was there any natural continuum between dense vegetation through bare soil (Phinn et al. 2002). Phinn et al. (2002) noted an only 43.57% accuracy for their overall classification of the area along the lines of V-I-S using per pixel classification. In comparison, VIS extracted from aerial photography provided better results, which was also due in part to its higher resolution. Here, the continuum between high/low dense areas was easier to distinguish as well the distinction of the different core V-I-S types.

Using a sub pixel method for classifying the same area, Phinn et al. (2002) noted an increased amount of detail and a greater degree of variability along the continuums but do not mention a direct measurably accurate comparison to the first two methods. While successful in describing the errors of a per pixel approach Phinn et al. (2002) were only able to allude to an increased accuracy using spectral unmixing and sub pixel VIS classification.

2.5: Advancing SMA Methods for Implementing Ridd's Model in Wu and Murray (2003)

While Phinn et al. (2002) were not able to provide a clear estimation of the accuracy sub pixel classification using spectral mixture analysis, Wu and Murray (2003) provided a much more clear justification of the use of spectral mixture analysis. Acknowledging the success by Ward et al. (2000) and Phinn et al. (2002) in applying the V-I-S model, Wu and Murray (2003) developed a methodology utilizing the fraction of four primary endmembers (vegetation, soil, low albedo and high albedo) calculated by a linear spectral mixture model (Wu and Murray 2003: p 494). While Wu and Murray (2003) address that a non-linear model should be used in cases where there is a very large scattered of photons that interact over a variety of different classification types, they assume that the scattering of photons over urban areas is negligible in “most urban” applications (Wu and Murray 2003: p 495) and reference Phinn et al. 2002; Rashed et al. 2001, and Small 2001, 2002, in which only linear spectral mixtures were used. The equation for linear spectral model used in Wu and Murray (2003) follows the framework: (Equation 1)

$$R_b = \sum_{i=1}^{N} f_i \, R_{i,b} + e_b$$

“where that R_b is the reflectance for each band b in the EMI+ image, N is the number of endmembers, f_i is the fraction of endmember i, $R_{i,b}$ is the reflectance of endmember i in band b, and $e_b$is the unmolded residual.” (Wu and Murray 2003: p 496). In addition it is required for determining R_b that $\sum_{i=1}^{N} f_i = 1$ and $f_i \geq 0$.

Using Landsat 7 ETM+ imagery converted from radiance to reflectance over the metropolitan area of Columbus, OH, Wu and Murray (2003) used a Maximum Noise Fraction (MNF) transformation to establish the endmember selection. Referencing the work by Green et al. (1988), they state that the MNF transformation “orders components [within the image] according to signal to noise rations” which can be used to identify Endmembers . Of the six MNF components of the ETM+ image, the first two MNF components are the most clear in illustrating the “spatially coherent contrasts differentiating CBD, residential areas, vegetation and water” (Wu and Murray 2003: p 496) while the third MNF components is crucial for distinguishing soil among other land cover types (Wu and Murray 2003: p 496). Using procedures developed by Smith et al.

(1985), Wu and Murray (2003) converted the MNF components into 2-D scatter plots (See Figure 7) and extracted the four-endmembers from the extreme pixel clusters.

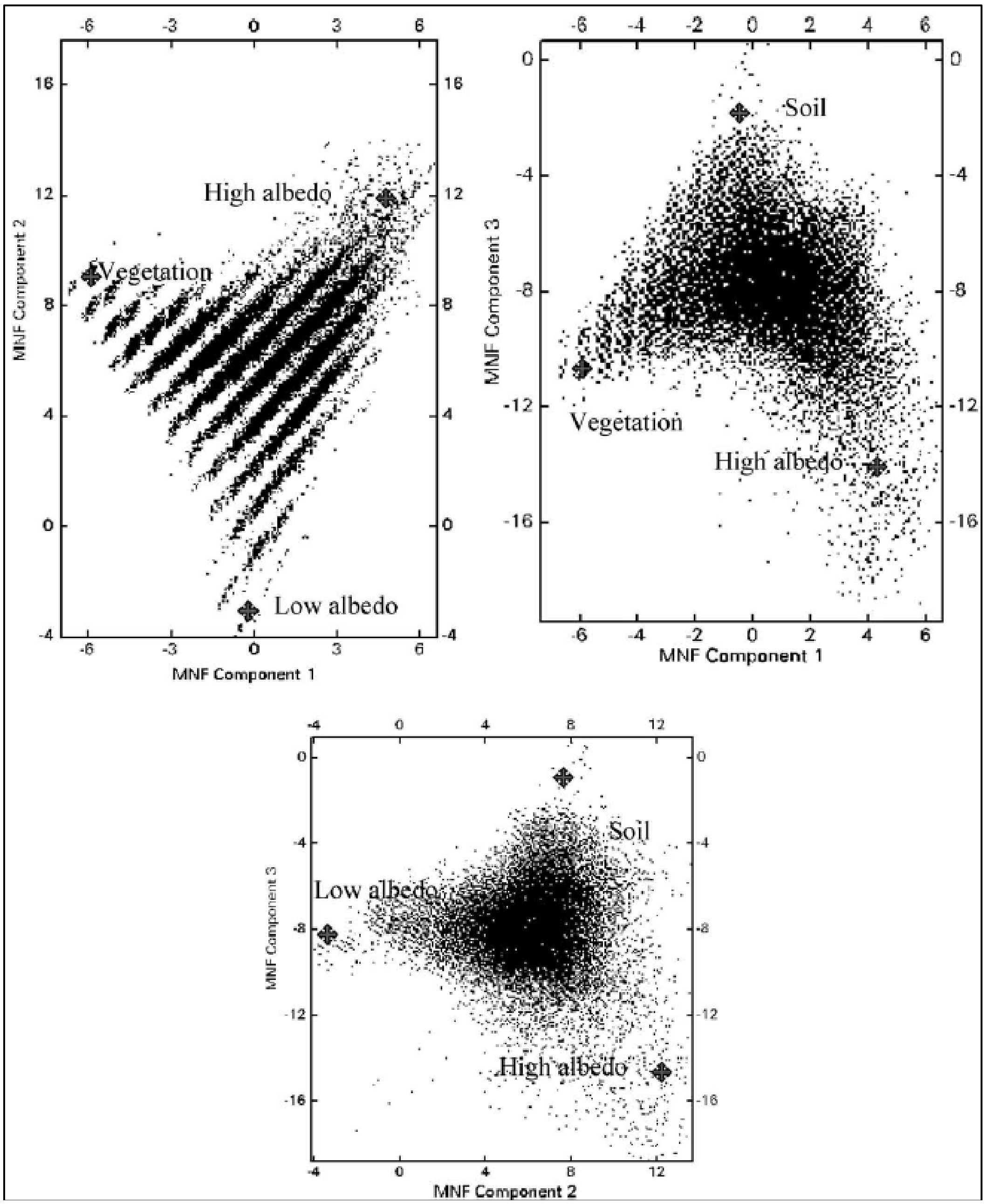

Figure 7: 2-D scatter plots from MFC components (Wu and Murray 2003: p 498)

Of the four-endmembers, the vegetation and soil are easy to conceptualize, but “the high albedo (e.g. concrete, clouds, and sand) and low albedo (e.g. water and asphalt)” (Wu and Murray 2003: p 497) are more difficult as they are comprised of very different components that have implications on how to utilize the V-I-S model. Additionally, Wu and Murray (2003) do not reference any other research with regards to the high/low albedo classification but rely on visual interpretation of the results of their MNF transformations. Admitting to issues with the selection of high albedo—due to low clustering and a possible nonlinear mixture between soil and high albedo— Wu and Murray (2003) state that they collected the endmember from “highly reflected roofs in the CBD because impervious surface is the most important in this study” (Wu and Murray 2003: p 947).

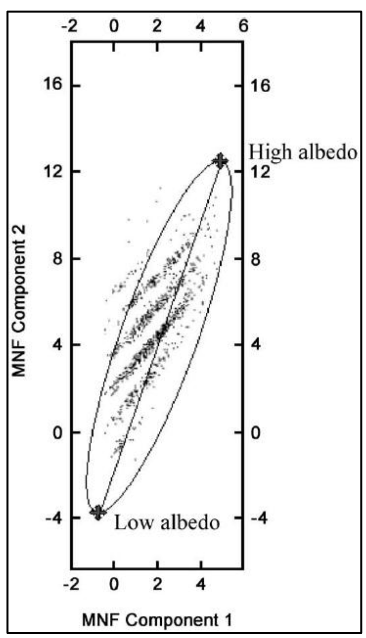

Figure 8: Linear relationship between high/ low albedos (Wu and Murray 2003: p 501)

Wu and Murray (2003) address the fact that high and low albedo endmembers cannot be used to directly interpret impervious surfaces, but through the analysis of the relationship between the high/low albedos, they determined that “impervious surfaces are likely to be on or near the line connecting the low albedo and high albedo endmembers,” (Wu and Murray 2003: p 499) which is described in their figure on the previous page(See Figure 8).

To test this relationship, Wu and Murray (2003) conducted a two-endmember unsupervised classification with both water and vegetation masked out over the CBD of their AOI, resulting in a mean RMS of 0.02 over all impervious surface pixels (being either on or within a small distance of the line between high and low albedo) (Wu and Murray 2003: p 499). Nevertheless, Wu et al. (2003) state: “some low reflectance materials (e.g. water and shade) and high reflectance materials (e.g. clouds and sand) adversely affect impervious surface estimation” (Wu and Murray 2003: p 499). However, in addressing the accuracy of developing a linear model to depict impervious surfaces from high and low albedo fractions, Wu and Murray (2003) report an overall estimated RMS of 10.6%. The one important note is that their model tends to overestimate impervious surface fraction in less developed areas while underestimating impervious surface fractions in the CBD (Wu et al 2003: p 502). Nevertheless, Wu and Murray (2003) clearly document a vast improvement of using sub pixel classification through spectral mixture analysis as opposed to earlier studies relying on per pixel classification.

Following the publication of Wu and Murray (2003), Wu (2004) expanded upon the methodology of using spectral mixture analysis for sub pixel classification of urban areas. In particular, Wu’s 2004 work set the methodology for normalizing the variations of brightness of the endmembers in order to increase the accuracy of surface estimation of the V-I-S model. In addition to the problems of extracting Endmembers caused by high and low albedo addressed in Wu and Murray (2003), Wu (2004) also references Asner (1998) in describing the variation of the spectral signature of green vegetation, such as differing leaf characteristics or canopy elements, that produce spectral 'dark vegetation' and 'bright vegetation.' Similarly, Wu (2004) describes the different types of soil that generate spectral variation depending on composition, grain size or water content, referencing Ben-Dor et al. (1999) and Irons et al. (1989), resulting in 'dark soil' and 'bright soil.' In addition, returning to Wu and Murray (2003), Wu (2004) also points to possible confusion between shade and low albedo materials and the recommendation for removal of shade using topological correction methods developed by Adams et al (1993). In order to address all of these issues, Wu proposes a normalized spectral mixture analysis (NSMA) model that would minimize the variations in brightness across all V-I-S endmembers.

2.6: Introduction of the Normalized SMA Process from Wu (2004)

Returning to the same study area over Columbus, OH from Wu and Murray (2003), Wu (2004) used a principal component (PC) transformation on the Landsat 7 ETM+ imagery to assist in endmember selection. PC transformation is a well-documented procedure to generate uncorrelated output bands that segregate noise components in order to identify the principal components of multispectral imagery, with Wu (2004) referring to Green et al. (1988), Rashed et al. (2001) and Small (2001), and can easily be calculated with programs such as ENVI or ERDAS. Similar to the methodology used in Wu and Murray (2003) to determine MNF fraction endmembers, Wu (2004) used 2-D scatter plots of the first three PC in conjuncture with visual interpretations of the original imagery to identify the breakdown of the variation of the V-I-S endmembers, as described in figure 9.

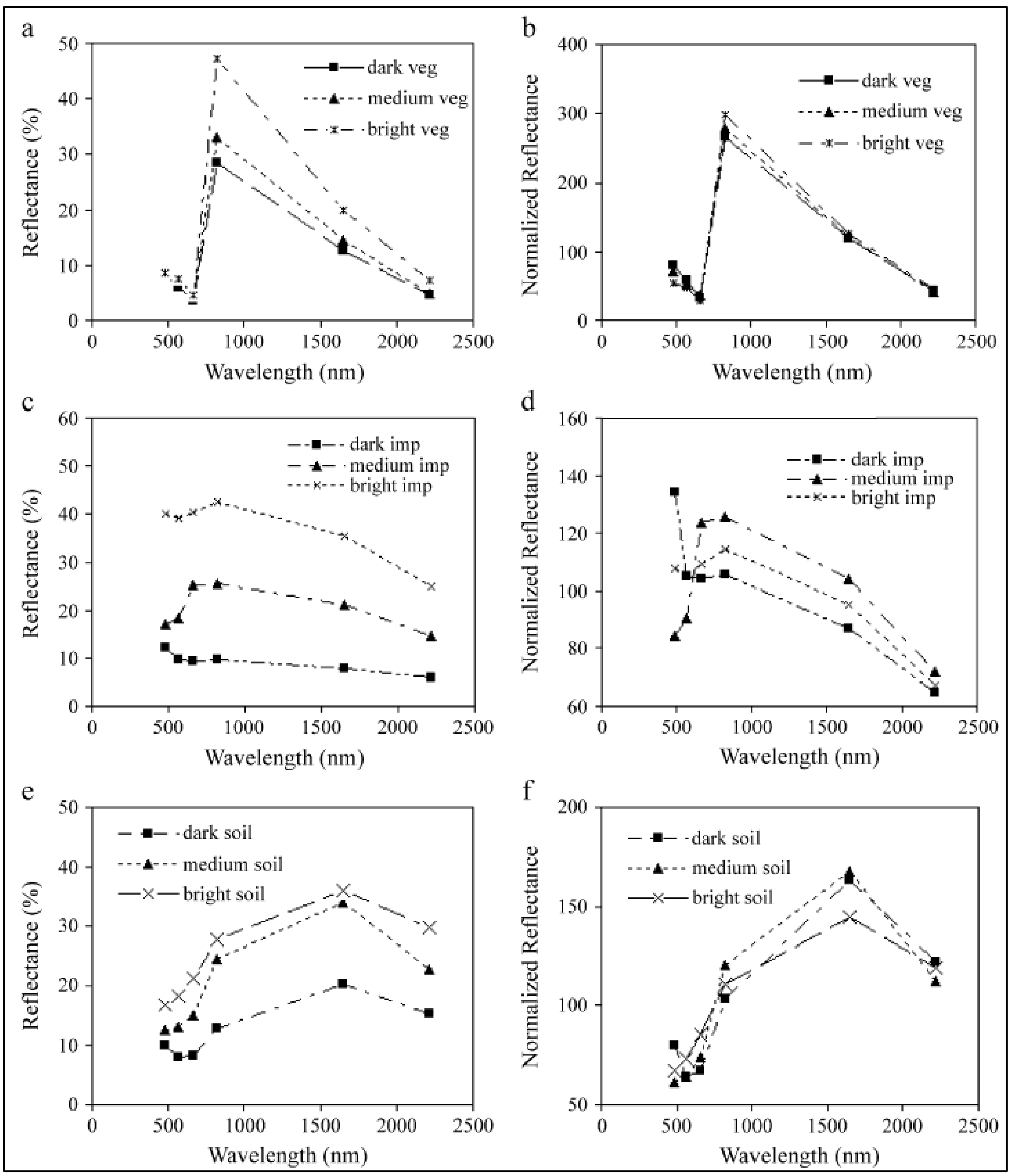

Figure 9: Brightness variation across Endmembers (Wu 2004: p 483)

Wu (2004) points out that although there is variation of brightness within the primary V-I-S components of the image, the overall structure or spectral shape of the bright, medium and low variants share common characteristics (although the % reflectance may change, the overall spectral form characterizes remain consistent across the different wavelengths), which again can be seen in figure 2.8 (Wu 2004: p 483-484).

In order to normalize the differences between the variations of the V-I-S components, Wu (2004) recommends a simple method of deriving the mean value across all bands of the ETM+ image and then normalizing (recalculating) the individual band per the mean as described in Wu's (2004) equation:

(Equation 2)

$$\{ \bar{R}_b = \frac{R_b}{\mu}\ x\ 100 \} \text{ where } \{ \mu = \frac{1}{N} \sum_{b=1}^{N} R_b \}$$

In this equation $\bar{R}_b$ is the normalized band generated as a ratio of the original band (R_b) over the mean (μ) multiplied by 100 and where the mean (μ) is the sum of all the individual bands divided by the total number of bands (Wu 2004: p 485). This equation for normalizing the bands is then applied to all the bands in the EMT+ image with the exception of band 6 (given that band 6 in Landsat TM and ETM+ images are typically ignored in all of these process as its spatial resolution is 120-m vs. the 30-m resolution of bands 1-5 and 7). While the normalization reduces the differences between the brightness of the V-I-S components across the image, Wu (2004) does make the important note that the process does cause significant loss of information. Other process, such as differentiating separate vegetation types (e.g. differentiating the individual signatures of two different types of trees) cannot be used with the normalized bands but it is still appropriate for creating the framework of Ridd's (1995) V-I-S model as only the three main components need to be distinguished (Wu 2004: p 485). Importantly, Wu (2004) states that the normalization process reduces the redundant information that causes errors in spectral mixture analysis and reports that first three components of PC transformation (computed against the normalized image) explain 99.7% of the total variances (Wu 2004: p486).

Following the normalization of the original EMT+ image, Wu (2004) use the same PC transformation to identify the groupings of the principal endmember to be used in the spectral mixture analysis, which was performed over the original image. Through visual inspection, Wu (2004) shows that the new fraction images produced by the NSMA process illustrate: "the distribution of vegetation, impervious surface, and soil correlates with their actual distribution in the [original] image" (Wu 2004: p 487). In order to compare the NSMA process to the original SMA process, Wu (2004) performed the SMA process against the original ETM+ image but used four-endmembers, incorporating 'shade' as a component to account for the components that could not be accounted for within vegetation, impervious surface or soil. The SMA process followed the same procedures as the linear model described in Wu and Murray (2003) for the four-endmember SMA:

(Equation 3)

{ $R_b = \sum_{i=1}^{N} f_i \, R_{i,b} + e_b$ } requiring that $\sum_{i=1}^{N} f_i = 1$ and $f_i \geq 0$.

With the same model used for the normalized bands ($\bar{R}_{b)}$:

(Equation 4)

{ $\bar{R}_b = \sum_{i=1}^{N} \bar{f}_i \, \bar{R}_{i,b} + e_b$ } requiring that $\sum_{i=1}^{N} \bar{f}_i = 1$ and $\bar{f}_i \geq 0$.

Performing an accuracy assessment against the NSMA and the SMA processes, Wu (2004) compared the fraction images against black-and-white aerial photographs (for both sets of composite images). The 'true' value used in the root mean square error (RMSE) and systematic error (SE) processes were derived from manually extracting the companion impervious surface values from the aerial photographs over the same sample sites and comparing them against the reported values of the NSMA and SMA processes. Wu (2004) reports that the normalized process produced an overall RSME of 10.1% while the four-endmember SMA produced an overall RSME of 18.3%. In addition, Wu (2004) also compared these values against the methods developed by Wu and Murray (2003), which in comparison reported a RSME of 22.2%, showing a direct improvement of the NSMA for predicting V-I-S over an urban area (Wu 2004: p 490). Diving deeper, Wu (2004) compared the three processes in less developed areas (% impervious surfaces is less than 30%) and more developed areas (% impervious surfaces is greater than 30%). Wu (2004) found that the NSMA produced better results in less developed areas with 6.1%, 9.1% and 26.6% RSME for NSMA, 4-Endmember SMA and Wu and Murray's SMA (2003) respectively. However, in more developed areas the NSMA was not as predictive as Wu and Murray's SMA (2003) with 14.5%, 27.5% and 11.7% for NSMA, 4-Endmember SMA and Wu and Murray's SMA (2003) respectively (Wu 2004: p 490). Calculating the SE, Wu's work showed that the NSMA tended to underestimate impervious surfaces with a -3.4 % SE, but which was not as much as the 4-Endmember SMA, with -10.8% SE, nor as much as the overestimation of Wu and Murray's SMA (2003), with +15.9% SE (Wu 2004: p 490).

Overall, Wu's research showed that normalizing the spectral bands prior to performing SMA reduced the problematic areas with the variation in reflectance between the core endmembers for the use in a standard V-I-S model. In particular, looking back to Ridd (1995), Ward et al. (2000), Phinn et al. (2002) Wu and Murray (2003), and Wu's (2004) approach is part of the logical evolution progression, moving away from per pixel classification to sub pixel classification, as well as the identification and correction of errors found between the variations of the primary vegetation, impervious surface and soil components. Although not a perfect, Wu's (2004) overall error rate is a significant decrease from the 63% accuracy in reported by Ward et al. (2000) and the 43.57% accuracy reported by Phinn et al. (2002).

2.7: Additional Examples of Urban Classification

Although not implemented in the methodologies for this work, additional studies since Wu (2004) have been conducted to improve the classification of urban areas using the V-I-S model. In particular, Lu and Weng (2006) address how surfaces temperatures derived from the thermal infrared band from Landsat ETM+ images (band 6) could be used to more accurately describe impervious surfaces for land-use classification. In their study, Lu and Weng (2006) use a nearest-neighbor algorithm to resample the 60-m by 60-m EMT+ band 6 to match the pixel size (30-m by 30-m) of the other bands. Utilizing the additional band, Lu and Weng (2006) utilize the same methodologies as Wu and Murray (2003) and Wu (2004) for spectral mixture analysis to generate fractional component images using four-endmembers: high albedo, low albedo, soil and vegetation. Lu and Weng (2006) used the resulting 4 component images generated through SMA to create 7 different land-use clarifications. While not strictly adhering to the V-I-S continuum, Lu and Weng (2006) primarily focused on four variations of residential land (low, medium, high and very high) with Commercial, industrial and transportation grouped into one classification, leaving “Non-urban lands” (vegetated areas and agricultural lands) and Water as the remaining classes. While Lu and Weng (2006) reported an overall classification accuracy of 87.38 and 83.78% for the first five classes (excluding Non-urban and Water) (Lu and Weng 2006: p 156), there is no direct assessment of how their model’s accuracy compares with the models generated by Wu and Murray (2003) and Wu (2004) who also look at addressing low/high albedos. While their methodology appears to produce interesting and accurate results, the use of the thermal infrared band was not used in this project.

2.8 Summary

A review of the literature shows that there has been a significant amount of research and work into the methods for classifying urban environments. From Weeks (2010) we started with the fundamental questions of how to define urban areas with regards to remote sensing. Within these settings, this work explored Ridd’s V-I-S model and how three endmembers can be graphically used to depict individual characteristics within the urban environment. Ward et al. (2000), show the of use of remotely sensed data to employ Ridd’s urban model is displayed, and is improved upon by moving to a sub pixel classification using SMA, shown in Phinn et al (2002). Wu and Murray (2003) take the methodologies used for classifying urban areas from SMA and explore how to improve the accuracy of extracting impervious surfaces through the linear relationship of high and low albedos. Most importantly for this work, the specific methods for normalizing the component bands that make up remotely sensed data prior to implementing SMA is well described in Wu (2004). While other works show how impervious surfaces can be used in various methods for depicting urban areas, this work will use the methods described in Wu (2004) for the normalized SMA process in implementing Ridd’s (1995) urban model.

CHAPTER 3: METHODOLOGY

3.1: Overview and Data

As the primary purpose of this project is to study the application of Ridd's (1995) V-I-S model using both Spectral Mixture Analysis and Normalized Spectral Mixture Analysis, the development of the methodologies follow closely the methods developed and described by Wu and Murray (2003) and Wu (2004). The data used in this project were derived from Level 1 Processed Landsat TM over Coban Guatemala, İzmit Turkey and Semey, Kazakhstan as well as the same Landsat ETM+ imagery used over Columbus Ohio by Wu and Murray (2003) and Wu (2004) which was used as a control site for this project. All Landsat images were downloaded directly from the United States Geological Survey (USGS) EarthExplorer server (http://earthexplorer.usgs.gov/).

Table 1: Landsat Data Info

CITY	ACQUISITION DATE	WRS PATH	STARTING ROW	ENDING ROW
COLUMBUS, OHIO	09/10/1999	19	32	32
COBAN, GUATEMALA	12/09/2009	20	49	49
İZMIT, TURKEY	08/13/2003	179	32	32
SEMEY, KAZAKHSTAN	08/17/2011	149	25	25

For this project, only the Landsat bands 1-5 and 7 were used, ignoring the 120 m resolution of band 6. While other projects resample band 6 to match the resolution of the other bands (Lu and Weng 2006), this project focus only on the same bands that were used by Wu (2004) in order to insure consistency. In addition, DigitalGlobe provided 2-meter multispectral imagery over the same AOIs (images taken within a 5 day period of the Landsat images). With regards to definitions to the Ridd's (1995) V-I-S model and their implications to the methods described: Vegetation (V) in this study follows Ridd's definitions of "green" vegetation, and Soil (S), or exposed soil, are combination surface components that do not fall within the classifications of impervious surfaces, vegetation, water or clouds. Impervious surfaces (I) are the manmade components of an urban area such as concrete, asphalt, roofing materials and other building components that are impervious to water.

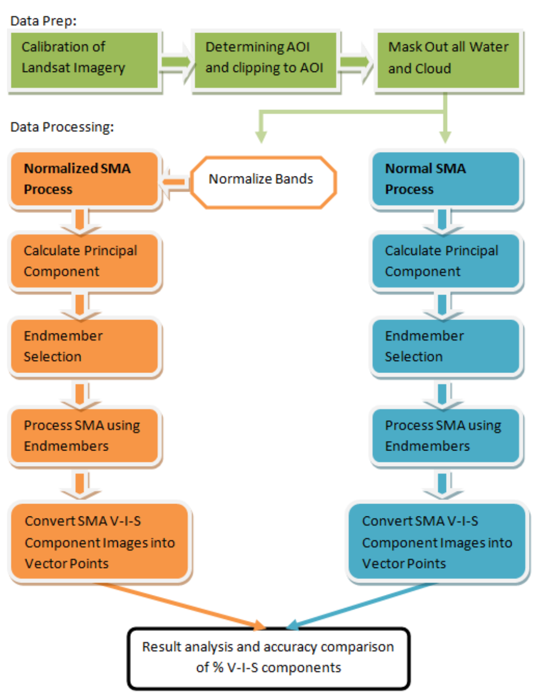

Figure 10: Methodology Flow Chart

3.2: Data Preparation

3.2.1: Calibration

The digital numbers (DN) of the TM and ETM+ images were converted to normalized exo-atmospheric reflectance. The equation for radiance to reflectance can be found in the Landsat 7 Science data user's handbook online (Irish 1998) seen in figures 11 and 12:

$$\rho_p = \frac{\pi \cdot L_\lambda \cdot d^2}{ESUN_\lambda \cdot \cos\theta_s}$$

Where:

ρ_p = Unitless planetary reflectance

L_λ = Spectral radiance at the sensor's aperture

d = Earth-Sun distance in astronomical units from an Excel file or interpolated from values listed in Table 11.4

$ESUN_\lambda$ = Mean solar exoatmospheric irradiances from Table 11.3

θ_s = Solar zenith angle in degrees

Figure 11: Reflectance to Radiance Equation
(http://landsathandbook.gsfc.nasa.gov/data_prod/prog_sect11_3.html)
Table 11.4 and Table 11.3 listed in Figure 10 can be found in the Landsat 7 Science Data Users Handbook through the hyperlink list above)

Where:

$$L_\lambda = ((LMAX_\lambda - LMIN_\lambda)/(QCALMAX - QCALMIN)) * (QCAL - QCALMIN) + LMIN_\lambda$$

where:	**L_λ**	= Spectral Radiance at the sensor's aperture in watts/(meter squared * ster * μm)
	Grescale	= Rescaled gain (the data product "gain" contained in the Level 1 product header or ancillary data record) in watts/(meter squared * ster * μm)/DN
	Brescale	= Rescaled bias (the data product "offset" contained in the Level 1 product header or ancillary data record) in watts/(meter squared * ster * μm)
	QCAL	= the quantized calibrated pixel value in DN
	$LMIN_\lambda$	= the spectral radiance that is scaled to QCALMIN in watts/(meter squared * ster * μm)
	$LMAX_\lambda$	= the spectral radiance that is scaled to QCALMAX in watts/(meter squared * ster * μm)
	QCALMIN	= the minimum quantized calibrated pixel value (corresponding to $LMIN_\lambda$) in DN = 1 for LPGS products = 1 for NLAPS products processed after 4/4/2004 = 0 for NLAPS products processed before 4/5/2004
	QCALMAX	= the maximum quantized calibrated pixel value (corresponding to $LMAX_\lambda$) in DN = 255

Figure 12: Definition of L_γ provided in the Landsat 7 Data Users Handbook (http://landsathandbook.gsfc.nasa.gov/data_prod/prog_sect11_3.html)

The conversion process from radiance to reflectance for all images was done using ENVI 5.0's Landsat Conversion toolset. ENVI's Landsat tool will automatic derive the necessary parameters for most of components of the equation given the input of the image capture date. However, it was noticed that ENVI sometimes incorrectly auto-populated the $LMin_\gamma$ and $LMax_\gamma$ (used to derive L_γ). As a result, all Landsat images being converted from radiance to reflectance had each parameter reviewed against the data header (*_MTL text file) provided from the USGS when the original Landsat datasets were downloaded and the corrections to the equations components were thus adjusted accordingly.

3.2.2: Determining AOI for SMA Processing

After each Landsat image was calibrated, the images were clipped to a standard AOI size for processing. In reviewing the original AOI used in Wu (2004), the county boundaries of Franklin County, Ohio, a standard 30 km by 30 km rectilinear polygon was centered on CBD of each city (1407 km^2 in Wu's (2004) study vs. 900 km^2 in this study). Each polygon was then used to clip all images for additional processing. An AOI of 30 km by 30 km was determined to be an appropriate size as given that it successfully encompassed the CBD for all cities as well as enough of the surrounding area to capture the spectral variations of the primary endmembers. Limiting the AOI to the city in question and its surrounding areas limits possible variants from other areas within the full scene Landsat image that could possible skew the SMA or Band normalization (many of the full scene Landsat images had significant cloud coverage in areas outside of the AOI)

3.2.3: Masking Out Water and Cloud Coverage

Although many studies have incorporated water as an endmember either at a per pixel level for land-use or land-type classification (Ward et al. 2000, Phinn et al. 2002), or at a sub pixel classification as part of SMA, this study chose to mask out all water and cloud converge in each AOI. Returning to the purpose of investigating Ridd's (1995) V-I-S model, Ridd (1995) clearly stated that water was ignored in developing the urban cover composition. Additionally, several works identified the issues of classifying urban areas using high albedo and low albedo as cloud and water spectral signatures can create confusion when determining impervious surfaces (Wu and Murray 2003, Wu 2004, Adems et al. 1993). Most importantly, as this project is using Wu's (2004) methodology for normalizing the Landsat bands, several tests were completed on the same Landsat images from Wu (2004) with water and clouds included, as well as with water and clouds masked out. This project could not successfully recreate Wu's (2004) results for normalized and raw SMA process without masking out water and clouds. Wu (2004) does not directly state if water and clouds were masked out or not. Attempts to contact Wu were unsuccessful. Additionally, initial investigation into the SMA process over other AOI's, in particular İzmit, Turkey, showed a significant amount of error during the SMA for extracting soil and impervious surfaces when water was not masked out. This was most likely due to what appears to be a large runoff of soil or other materials into the Sea of Marmar from the major river that runs through the city.

Using ENVI, a NDVI over NIR image was created to quickly distinguish water and clouds pixels from non-water or non-cloud pixels. This was particularly helpful in the area surrounding Coban, Guatemala as several of the small water bodies in the dense vegetation were not immediately located during a visual inspection. From this image a Region of Interest (ROI) of all water and cloud pixels was created for each AOI. This ROI was then edited using visual interpretation of the images to locate any additional water or cloud pixels. The ROI was then converted into an ENVI mask image which was then applied to the AOI.

3.3: Data Processing

3.3.1: Band Normalization

The band normalization process follows the process set up by Wu (2004). Using the calibrated, clipped and masked image over each AOI the band mean was derived from bands 1-5 and 7 utilizing ENVI's band math tools. Once the mean was derived, each individual band was normalized per Wu's (2004) equation explained in the literature review (See Equation 2 on page 32). These normalized bands were then set up as a combined image for the SMA process in the same manner as the original image.

3.3.2: Principal Component Calculation

The principal components for each dataset (raw and normalized) over each AOI were calculated using EVNI's Principal Component Forward Transformation toolset. The result of the PC transformation were six component images relating to their eigenvalue number (percentage of data variance) in each component (the first component image having the largest percentage of data variance with the second component image having the second largest percentage of data variance, and so on). In all cases, the number of components needed to describe the variance in the images dropped in the normalized images.

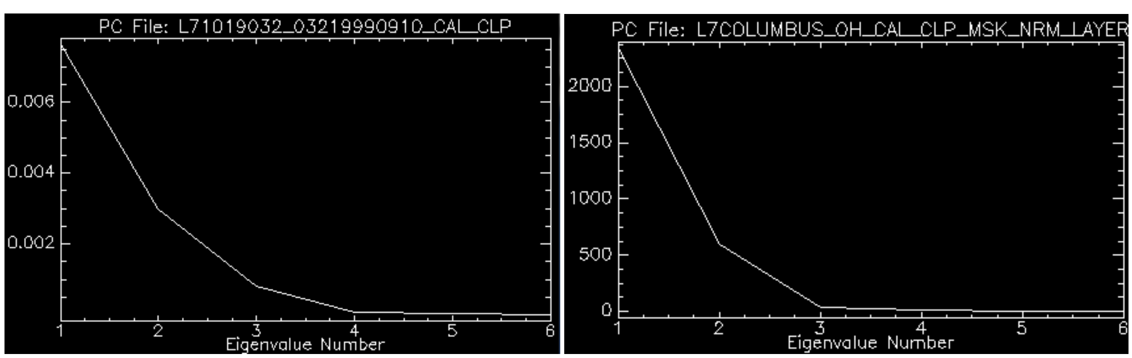

A. Raw B. Normalized

Figure 13: Columbus, Ohio Eigenvalue numbers

As seen above in Figure 13 the number of Eigenvalue numbers shifted strongly from 4 to 3 with Wu’s (2004) normalization.

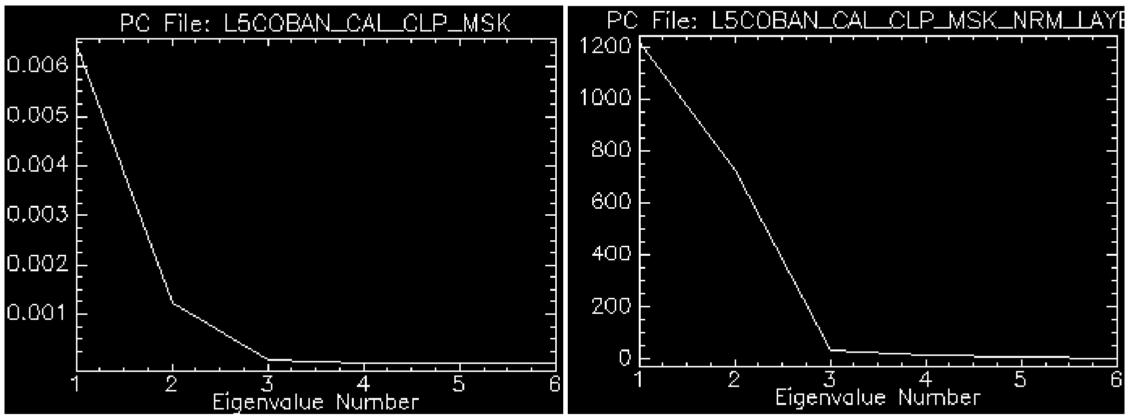

A. Raw B. Normalized
Figure 14: Coban, Guatemala Eigenvalue numbers

As seen in Figure 14, Coban was the only site that saw an increase in the percentage of variance reported by the second component image after the bands were normalized. This is important to note, as this implies that the prominence of the second component images describes more of the overall scene after being normalized than it did prior to being normalized. All AOIs saw a decrees in percent variance reported in the second and third component images.

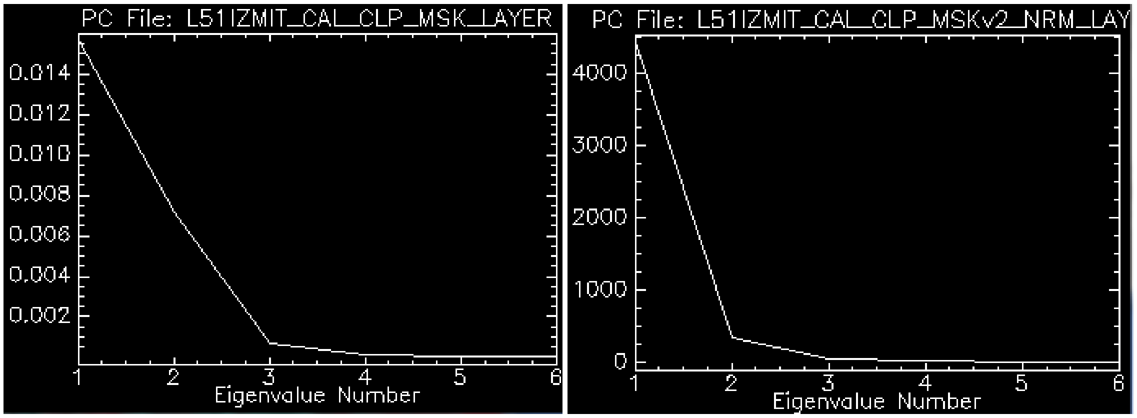

A. Raw B. Normalized

Figure 15: İzmit, Turkey Eigenvalue numbers

As seen in Figure 15, Wu's (2004) normalization had less of an effect on the overall number of primary components that we need to describe the images; however it did significantly decrease the strength of the second component in describing the image.

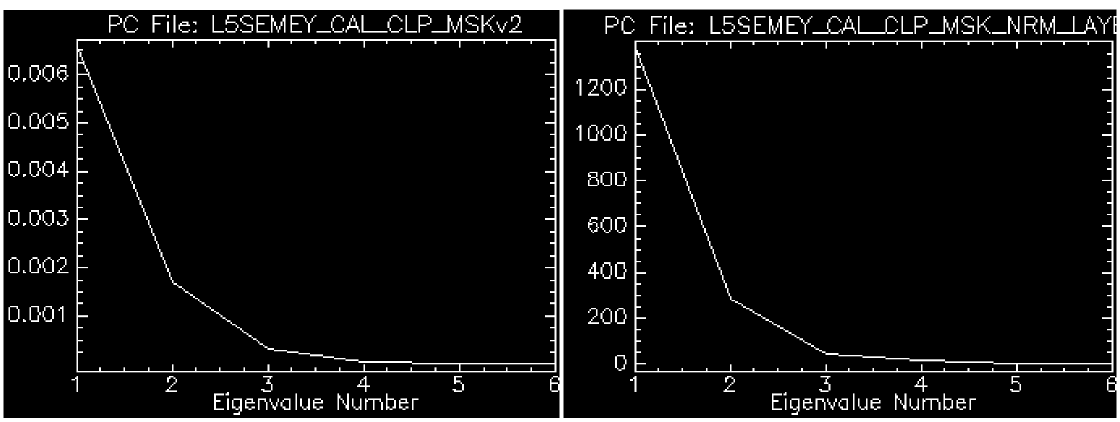

A. Raw B. Normalized

Figure 16: Semey, Kazakhstan Eigenvalue numbers

As seen in in Figure 16, Wu's (2004) normalization had a less impact in the primary components over Semey in comparison to the other cities. However, the first three primary components describe the vast majority of imagery over Semey.

3.3.3: Endmember selection

Given that the Eigenvalue numbers report, which indicates that the first three PC component images explain over 95% of the variations in the original image, this work used the first three PC component images to create 2-D scatter plots for both raw and normalized datasets. In ENVI, these 2-D scatter plots were linked back to the images they were derived from in order to visually verify the type of components they represented. Endmembers representing vegetation, impervious surfaces and soil were taken from the mean spectral signatures from the clustering of the 2-D scatter plots. These endmember groupings are seen in figures 17 and 18 for Columbus, 20 and 21 for Coban, 23 and 24 for İzmit and 26 and 27 for Semey.

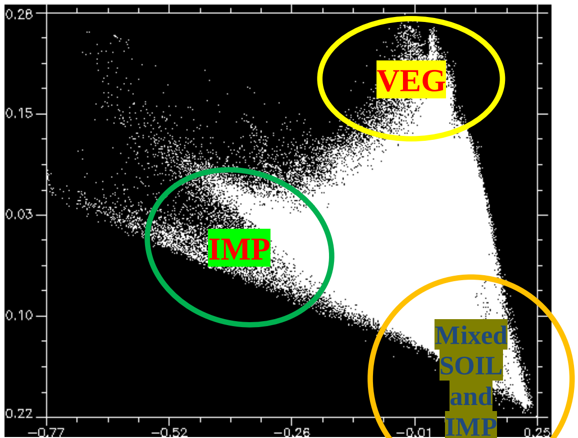

A: X-axis: PC 1 / Y-axis: PC 2

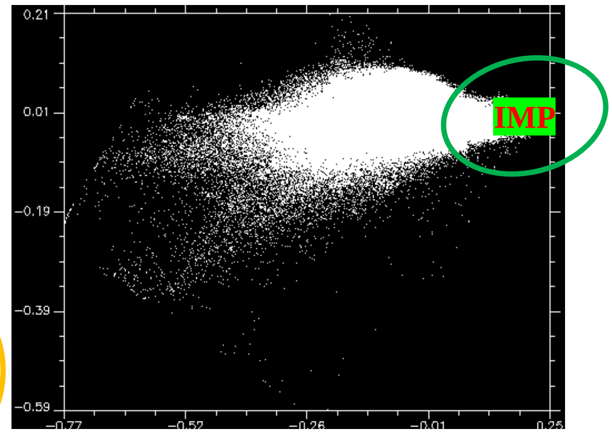

B: X-axis: PC 1 / Y-axis: PC 3

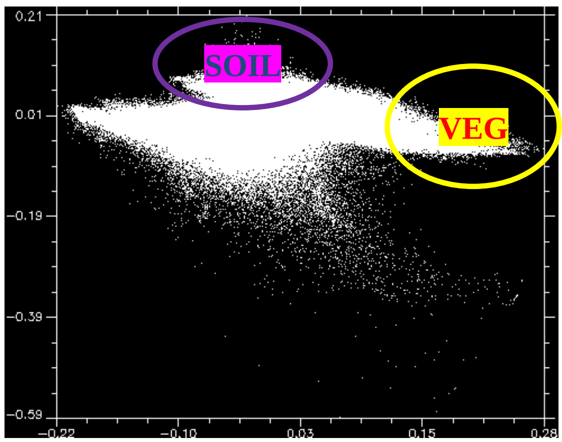

C: X-axis: PC 2 / Y-axis: PC 3

Figure 17: Columbus, Ohio Raw PC Components

Here in Figure 17, the clustering of the different primary components could be used to identify the three Endmembers for Vegetation, Impervious Surface and Soil for Columbus, Ohio. The grouping of these primary components were also compared against a composite image using Landsat bands 5, 4, and 2 to help differentiate between vegetation and impervious surfaces. Given the known issues of high and low albedo that can cause classification differences between impervious surfaces and soil, only areas that best represented the endmembers were extracted through visual interpretation of the imagery.

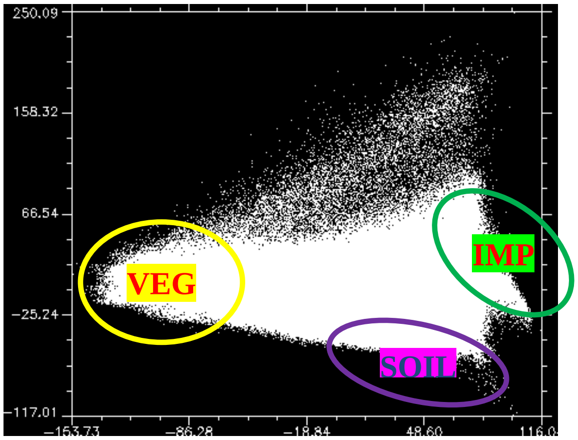

A: X-axis: PC 1 / Y-axis: PC 2

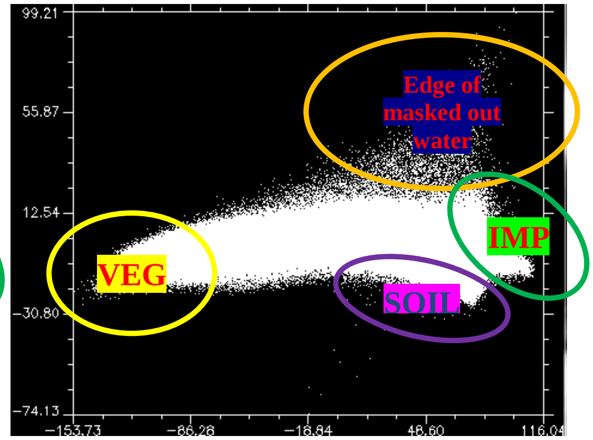

B: X-axis: PC 1 / Y-axis: PC 3

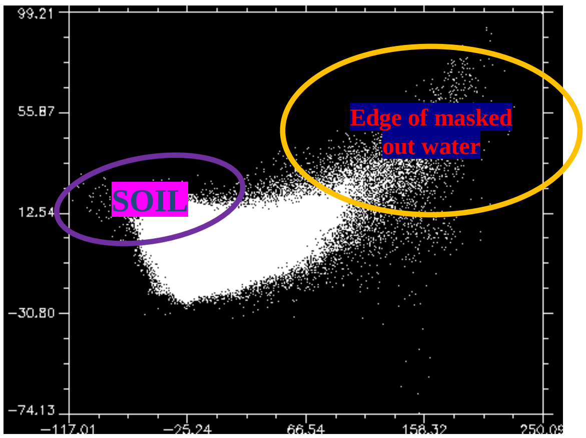

C: X-axis: PC 2 / Y-axis: PC 3

Figure 18: Columbus, Ohio Normalized PC Components

In comparison, the groupings of the endmembers within normalized PC components were easier to differentiate. However, there were larger sections (as seen in Figure 18) of the clustering of “errors,” which were identified as the areas along edge of the sections of water and clouds that were masked out.

From the endmember selection, the mean values of the individual points that depicted the 'ideal' endmembers were captured for use in SMA process. Figure 19 shows the comparative wavelengths between the raw and normalized Endmembers. Although there was some slight change in the spectral shape, the overall shapes remained constant for all Endmembers.

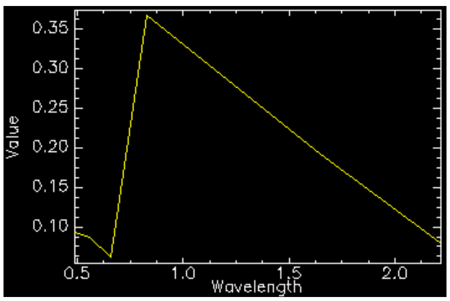

A: Raw Vegetation Signature

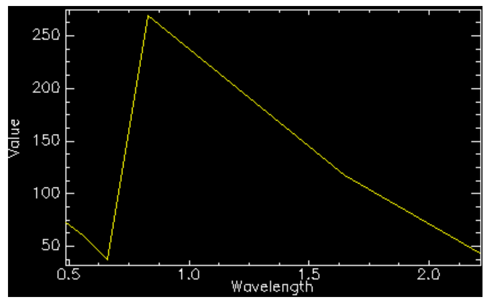

B :Normalized Vegetation Signature

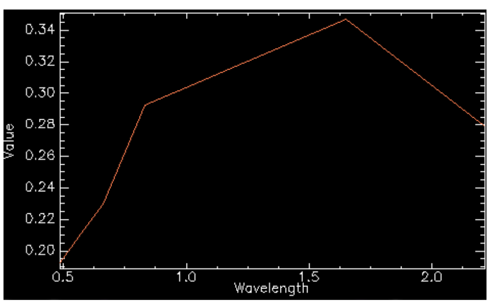

C: Raw Impervious Surface Signature

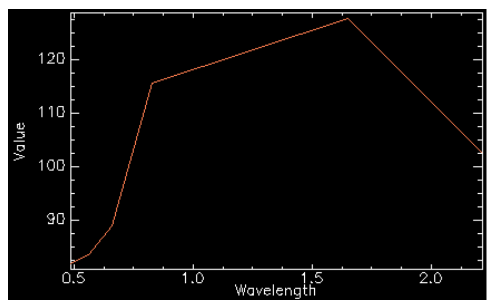

D: Normalized Impervious Surface Signature

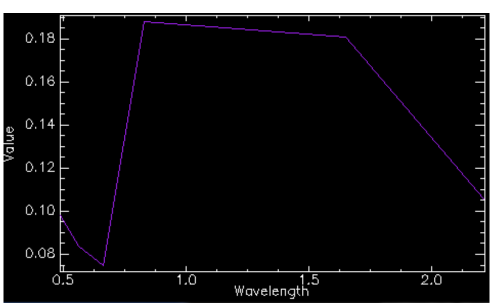

E: Raw Soil Signature

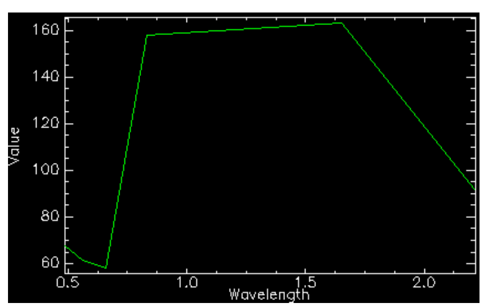

F: Normalized Soil Signature

Figure 19: Spectral Signatures for Columbus Ohio

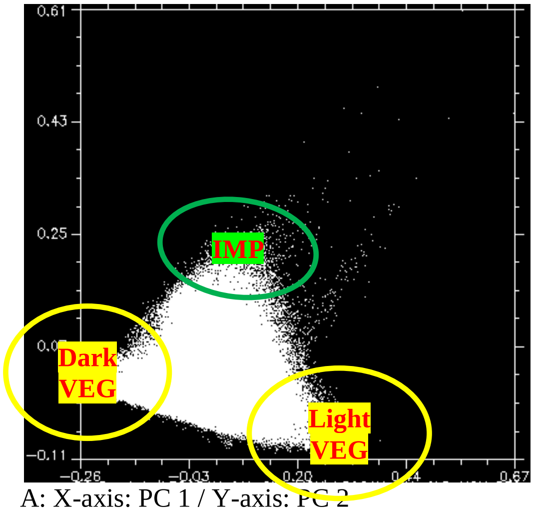

A: X-axis: PC 1 / Y-axis: PC 2

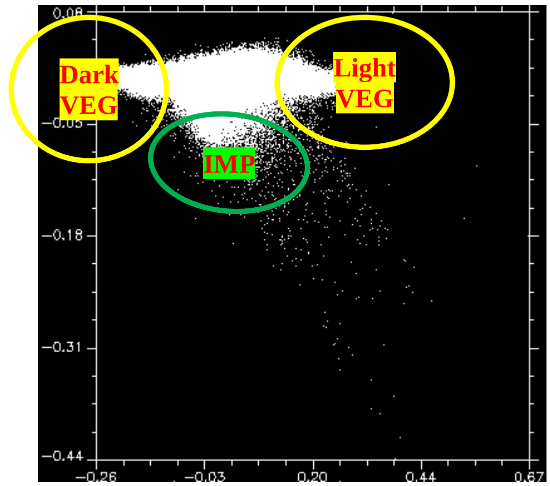

B: X-axis: PC 1 / Y-axis: PC 3

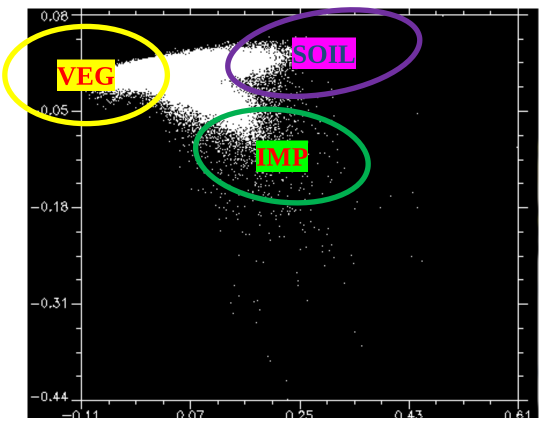

C: X-axis: PC 2 / Y-axis: PC 3

Figure 20: Coban, Guatemala Raw PC Components

The Endmember selection for Coban was slightly more difficult, as the clustering of the primary Endmembers showed a strong difference between dark vegetation and light vegetation. The mean value of the dark and light vegetation was used as the Endmember for vegetation. Additionally, all the Endmember (in particular that for Soil) were also confirmed by visually comparing the resulting clustering of the 2-D scatter plot against the DigitalGlobe imagery to correctly identify soil, or exposed surfaces as opposed to the surrounding vegetation and impervious surfaces.

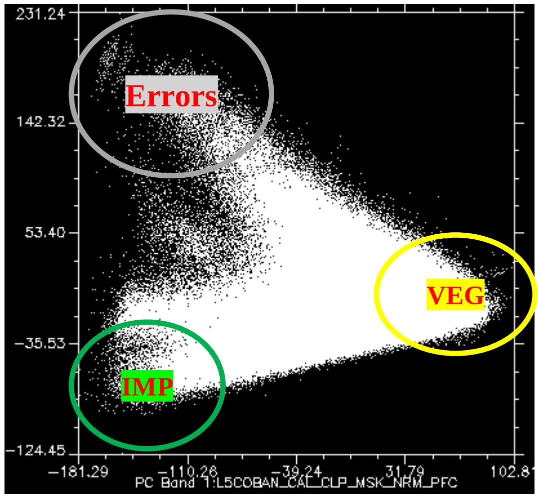

A: X-axis: PC 1 / Y-axis: PC 2

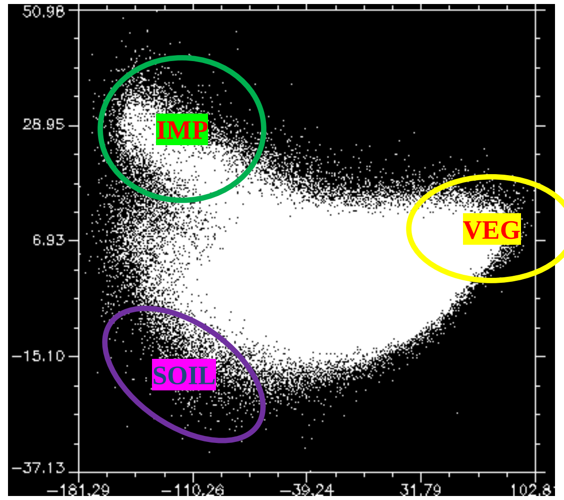

B: X-axis: PC 1 / Y-axis: PC 3

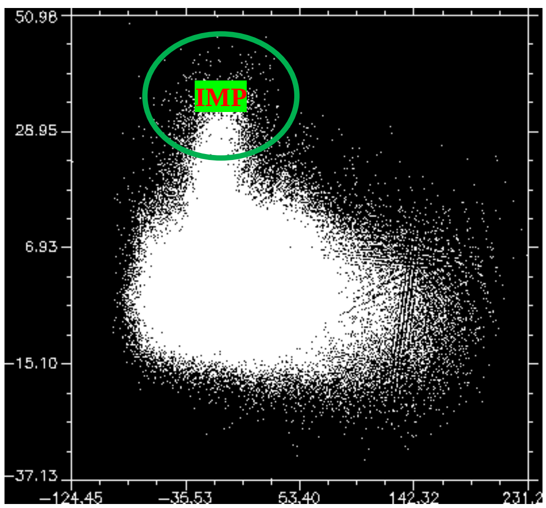

C: X-axis: PC 2 / Y-axis: PC 3

Figure 21: Coban, Guatemala Normalized PC Components

Seen in Figure 21, the normalized PC components showed that the bright and dark vegetation for Coban were collapsed into the same clustering (the intention of the normalization). Soil was slightly more easily identified from impervious surfaces, however it still needed to be confirmed against the DigitalGlobe imagery. As in Columbus, the areas around the edge of the masked out water clustered a larger amount of the errors found within the image. These were sections that that could be confused with either soil or impervious surfaces. The wavelengths of the Endmembers for both the raw and the normalized images that were used in the SMA process can be seen in Figure 22.

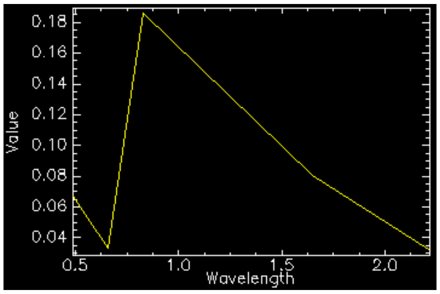

A: Raw Vegetation Signature

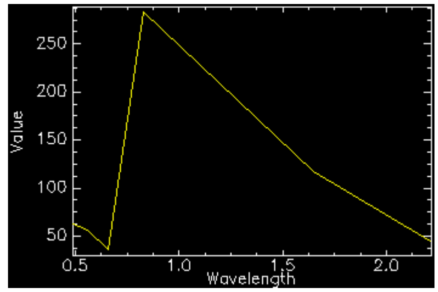

B: Normalized Vegetation Signature

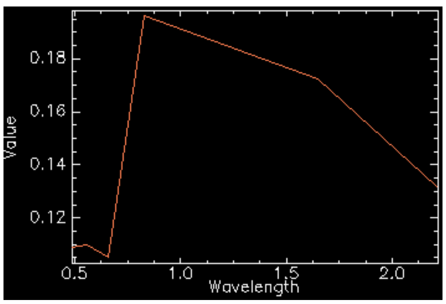

C: Raw Impervious Surface Signature

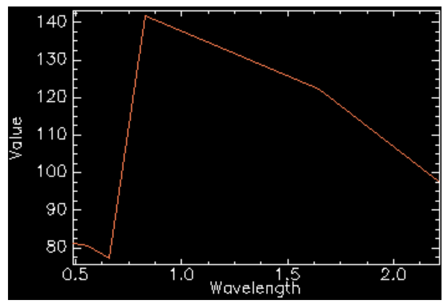

D: Normalized Impervious Surface Signature

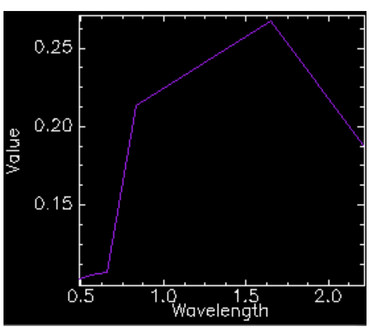

E: Raw Soil Signature

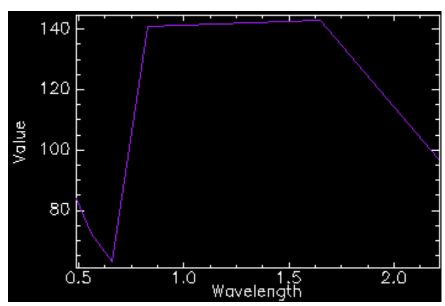

F: Normalized Soil Signature

Figure 22: Spectral Signatures for Coban, Guatemala

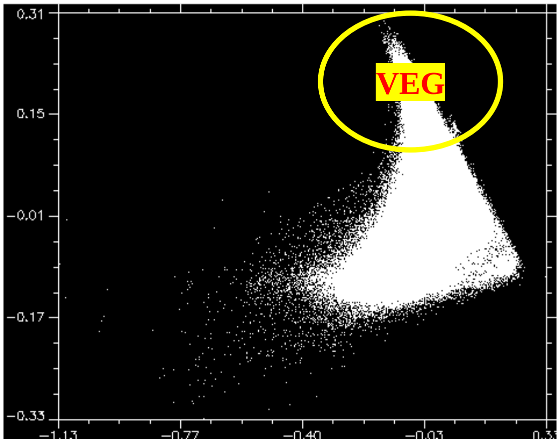

A: X-axis: PC 1 / Y-axis: PC 2

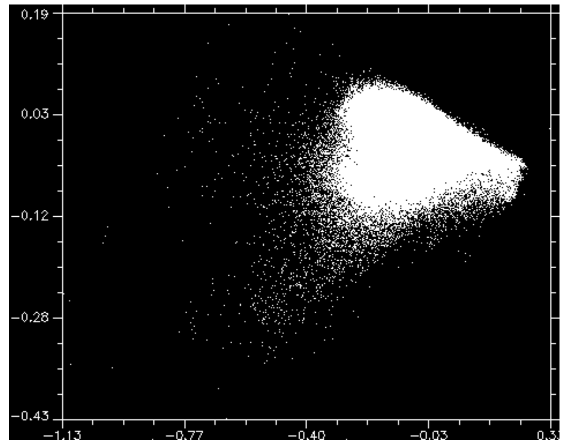

B: X-axis: PC 1 / Y-axis: PC 3

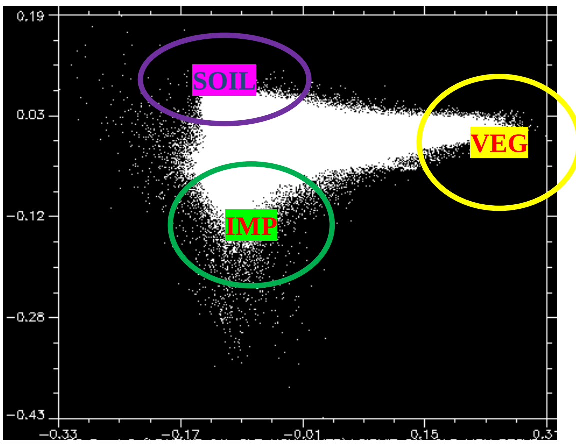

C: X-axis: PC 2 / Y-axis: PC 3

Figure 23: İzmit, Turkey Raw PC Components

Out of all the all the sites, the Endmembers were easiest to extract from the raw PC components from İzmit, Turkey. During an investigation stage of the imagery over İzmit, the PC transformation was applied without first masking out the water and clouds. In this case, it was much more difficult to differentiate soil from impervious surfaces.

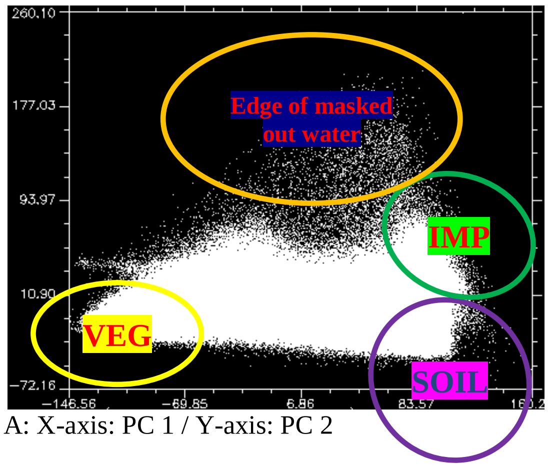

A: X-axis: PC 1 / Y-axis: PC 2

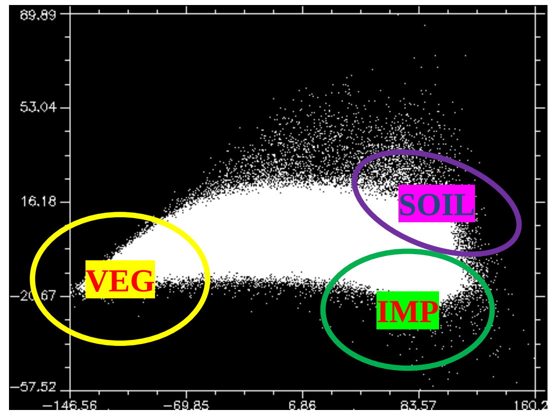

B: X-axis: PC 1 / Y-axis: PC 3

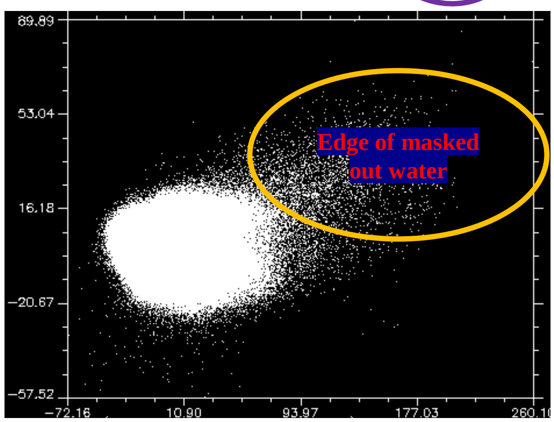

C: X-axis: PC 2 / Y-axis: PC 3

Figure 24: İzmit, Turkey Normalized PC Components

In comparison to the raw PC transformation, the normalized PC components provided more of a challenge to identify correct clustering, all of which needed to be verified with the DigitalGlobe imagery. The 2-D scatter plot of PC 2 / PC 3 (see Figure 24.C) was unable to provide any ‘pure’ or best-for-sue endmembers as the vegetation, impervious surfaces and soil were too closely group together.

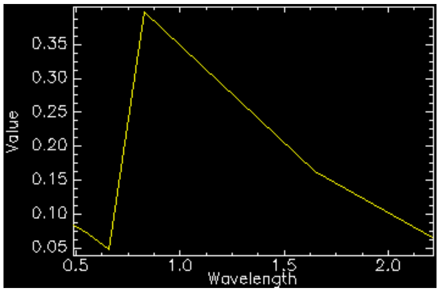

A: Raw Vegetation Signature

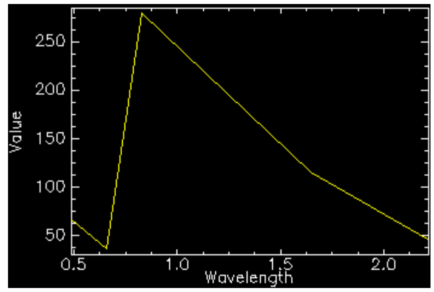

N: Normalized Vegetation Signature

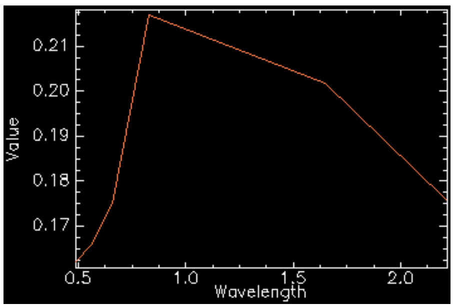

C: Raw Impervious Surface Signature

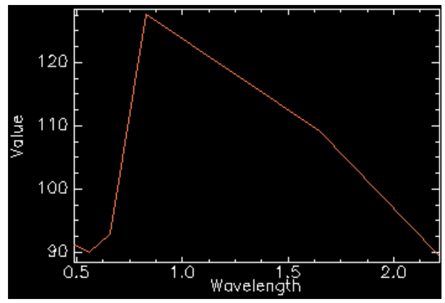

D: Normalized Impervious Surface Signature

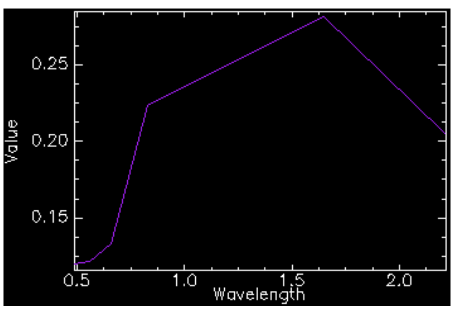

E: Raw Soil Signature

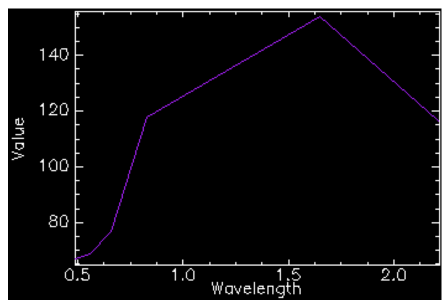

F: Normalized Soil Signature

Figure 25: Spectral Signatures for İzmit, Turkey

Similar to all sites, the overall change in the spectral shape of the endmembers used in the SMA process was very small.

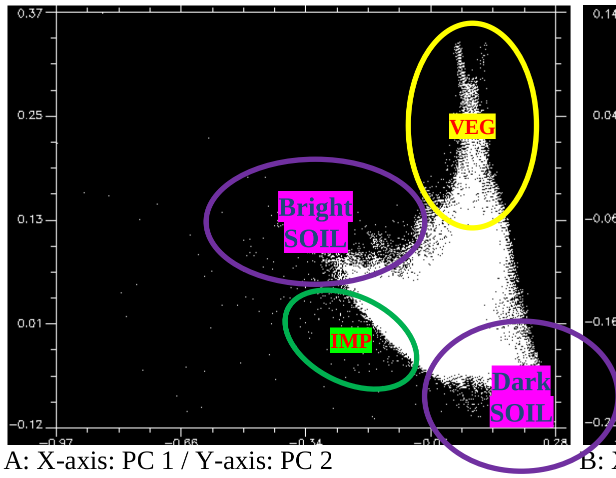

A: X-axis: PC 1 / Y-axis: PC 2

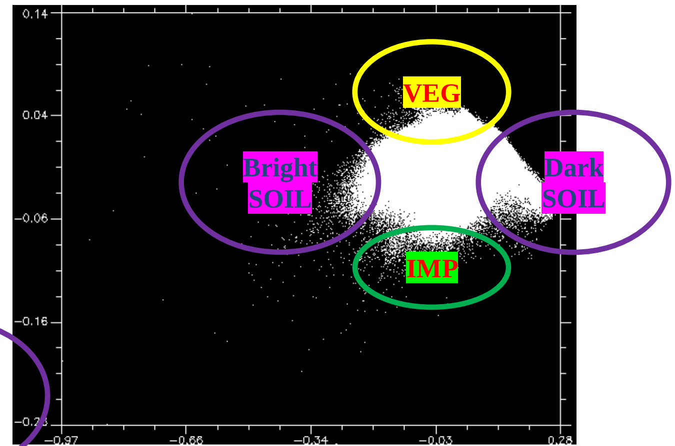

B: X-axis: PC 1 / Y-axis: PC 3

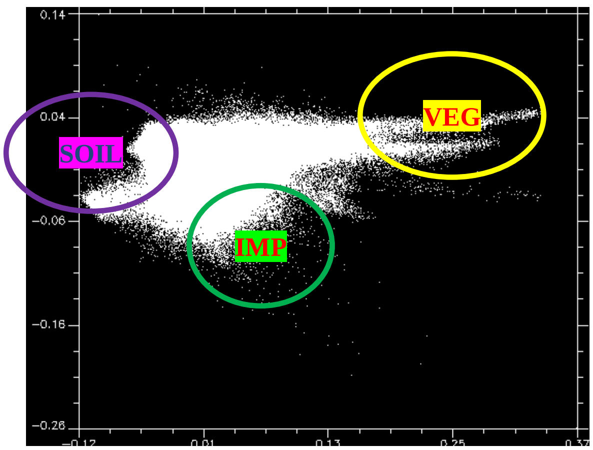

C: X-axis: PC 2 / Y-axis: PC 3

Figure 26: Semey, Kazakhstan Raw PC Components

Similar to the differences between bright and dark vegetation in Coban, the raw PC transformation for Semey showed a large variation in brightness between one of the primary Endmembers. However, in Semey, the variation was between bright and dark soil (exposed surfaces). Careful visual inspection of the Endmembers in comparison of the DigitalGlobe imagery was also highly needed as the bright and dark soil formed clusters around areas of impervious surfaces.

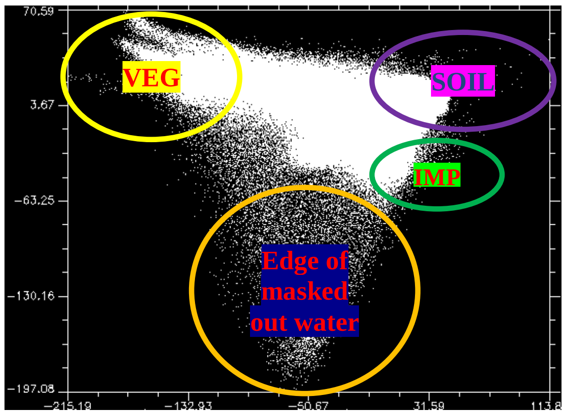

A: X-axis: PC 1 / Y-axis: PC 2

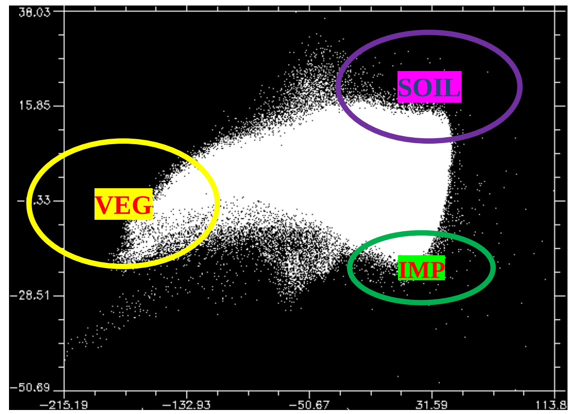

B: X-axis: PC 1 / Y-axis: PC 3

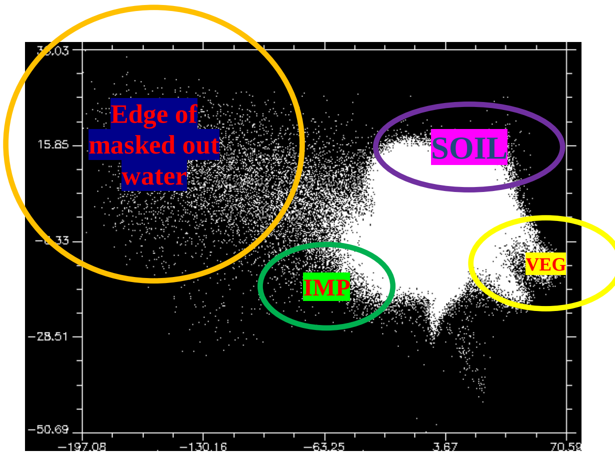

C: X-axis: PC 2 / Y-axis: PC 3

Figure 27: Semey, Kazakhstan Normalized PC Components

In comparison to the raw PC components for Semey, the normalized PC components made it easier to differentiate the soil and impervious surfaces. As with Coban, the variations in brightness were dramatically reduced in the normalization process. However, as with all other sites, the normalized process also clustered the ‘errors’ around the edges of the masked out water. Although easier to differentiate, the Endmembers for the normalized components were also compared against the DigitalGlobe imagery.

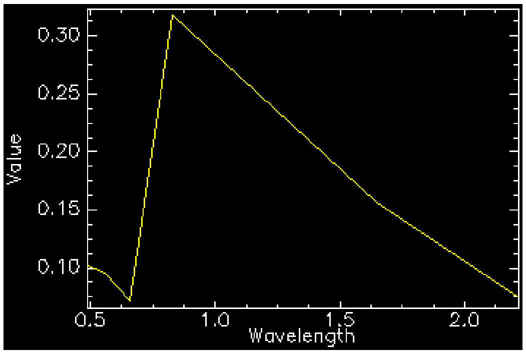

A: Raw Vegetation Signature

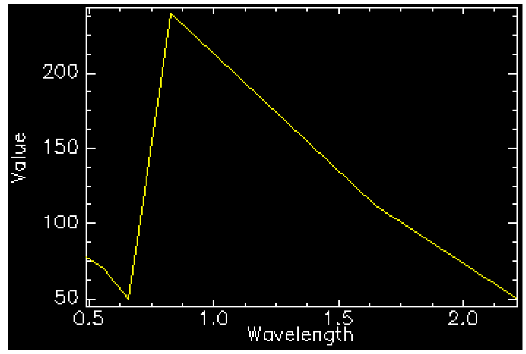

B: Normalized Vegetation Signature

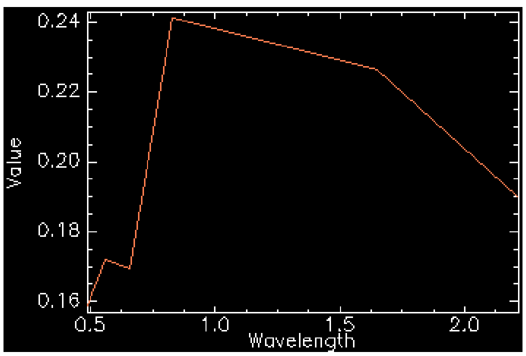

C: Raw Impervious Surface Signature

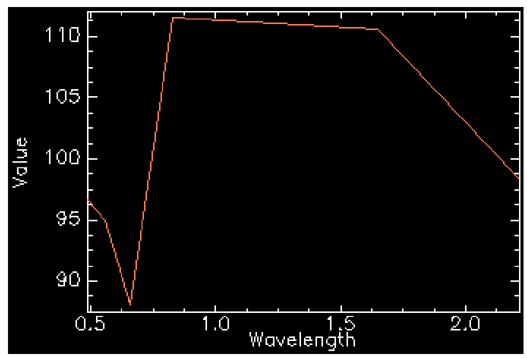

D: Normalized Impervious Surface Signature

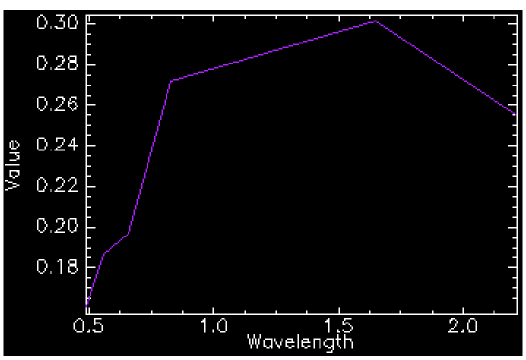

E: Raw Soil Signature

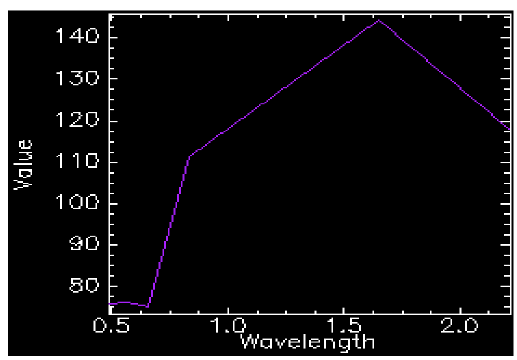

F: Normalized Soil Signature

Figure 28: Spectral Signatures for Semey, Kazakhstan

The specular signatures of the Endmembers for Semey (seen above in figure 28) showed the same consistency of the basic spectral shape across the raw and normalized Endmembers. However, Semey saw a large variation of the endmember between raw and normalized impervious surfaces in comparison to the other cities. This variation could not be explained and additional research would be needed to address this.

3.3.4: Processing SMA using Endmembers

The same linear spectral model from Wu and Murray (2003) and Wu (2004) was applied to all AOIs for both raw and normalized datasets.

{ $R_b = \sum_{i=1}^{N} f_i R_{i,b} + e_b$ } requiring that $\sum_{i=1}^{N} f_i = 1$ and $f_i \geq 0$. R_b for raw bands being replaced by $\bar{R}_b$ for normalized bands.

The SMA was processed using ENVI's Linear Spectral Unmixing toolset, using the endmembers identified through the PC transformation and visual interpretation described earlier. The result of the SMA process were component images corresponding to endmember classes with each pixel representing the abundance of the endmember as an error component image (e_b) showing how well all the pixels could be described using the endmembers provided.

3.3.5: Convert SMA V-I-S Component Images to Vector Points

Using the component images processed by ENVI's linear spectral unmixing, each image was converted into a vector class (points) to allow for quicker manipulation and calculations for analysis. The conversion from raster to vector was processed using ESRI's ArcMap's Conversion Tools 'Raster to Point' toolset, where the 0-255 grayscale value for each pixel of the component images was transferred as the value for point (each pixel collapsing to a single point located at the center of the pixel). The resulting points derived from the component images were then collapsed into a single point class. While not necessary, having a single point class maintaining the individual V, I, S and error values as well as storing any additional calculations based on the combinations of the values, allowed for faster analysis and comparison.

3.4: Additional Processing

During the endmember selection and SMA process, it became evident that for Coban, Guatemala and Semey, Kazakhstan that using a raw 3-endmembers (V-I-S) SMA produced too many errors. Due to the unique spectral variations in the surrounding environments, a raw 4-endmember SMA was processed in addition to the raw 3-endmember and 3-endmember normalized SMA processes. In particular, in Coban vegetation (V) was broken into two-endmembers representing bright vegetation and dark vegetation, while in Semey soil (S) was broken down into two-endmembers representing bright soil and dark soil.

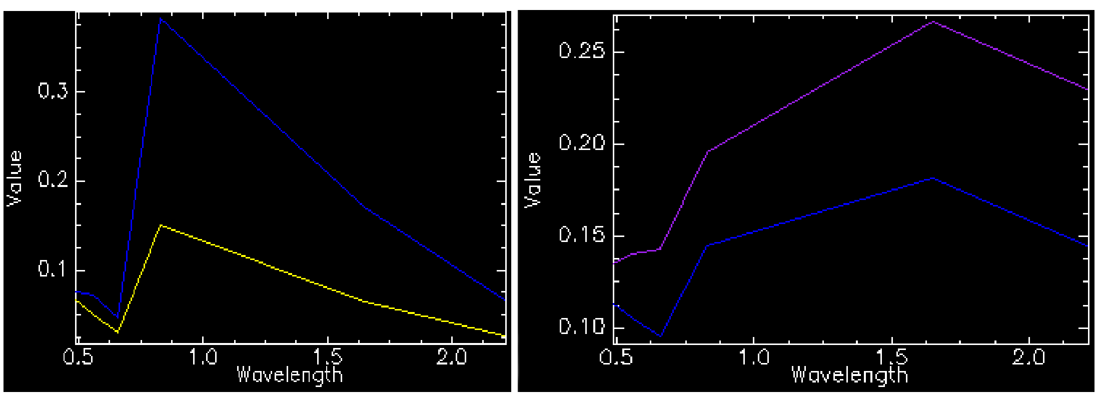

A. Raw Vegetation (Coban, Guatemala) B. Raw Soil (Semey, Kazakhstan)
Figure 29: Endmembers processed as two Endmembers. A: Bright (Blue) and Dark (Yellow) Vegetation for Coban, Guatemala and B: Bright (Purple) and Dark (Blue) Soil for Semey Kazakhstan.

CHAPTER 4: RESULTS

4.1: Overview

The results for each SMA process were compared in tandem against high resolution satellite imagery provided by DigitalGlobe across the AOIs. The accuracy assessment was broken into two categories:

1. Impervious surface estimation of the SMA process versus ‘true” impervious surfaces collection from DigitalGlobe imagery through visual inspection,
2. Site composition across the V-I-S continuum, to assess the accuracy of how well the V-I-S model described the Rural-Urban continuum.

With regards to the first accuracy assessment, the methodology used to determine the accuracy of the impervious surface estimation followed the same basic procedure as how Ridd (1995), Ward et al. (2000), Phinn et al. (2002), Wu and Murray (2003) and Wu (2004) reported the accuracy of their models and research. Delineating the “observed” when calculating observed versus expected impervious surfaces error rate is much easier to accomplish using high resolution imagery as a control. Conducting “on-site” ground truth measurements for the four AOIs in this project in order to establish “true” soil and vegetation was not practical or feasible. In addition, none of the other authors of the pre-mentioned works address the direct accuracy of vegetation or soil estimation through the SMA process. However, the overall accuracy of the how well the V-I-S model describes and area can be inferred through visual inspection. This project does did not assess the accuracy of the impervious surface estimation over Columbus, Ohio, as the aerial photography used by Wu and Murray (2003) and Wu (2004) was not available. Visual comparison of this projects processing of the Columbus, Ohio data and Wu's (2004) results indicate that they are comparable.

4.2: Accuracy Assessment: Impervious surface estimation

The accuracy assessment of the impervious surface estimation follows the same procedures as described in Wu (2004), which are similar to the procedures in Phinn et al. (2002), Ward et al. (2000) and Wu and Murray (2003). Ninety sample locations were reviewed in each AOI, with the samples being grouped into 3x3 pixel clusters in order to reduce the influence of possible geometric errors from the original Landsat imagery and to reduce possible variance caused through the SMA process. The observed value of impervious surface was taken as the mean value of the 9 pixels within the 3x3 area, while the expected value of impervious surface was extracted through visual interpretation of the DigitalGlobe imagery (See figure 30).

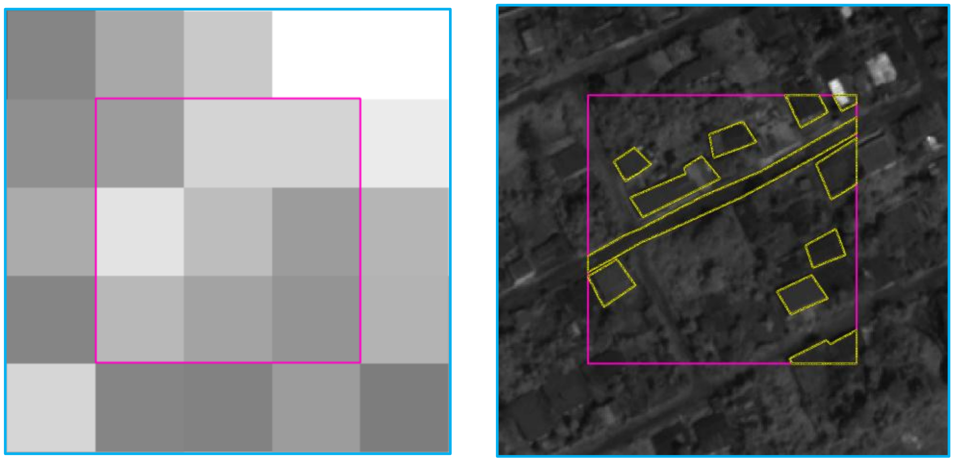

A. Landsat B. DigitalGlobe

Figure 30: Sample accuracy assessment site with 29.A showing the 3x3 pixels from the resulting impervious surface image from the 3-endmember SMA process and 29.B shows the visual interpretation of impervious surfaces from DigitalGlobe panchromatic imagery, both over Coban, Guatemala.

High resolution panchromatic imagery and multispectral imagery was available in Coban, Guatemala, while only high resolution multispectral imagery was used over İzmit, Turkey and Semey, Kazakhstan. Once the expected impervious surfaces were extracted from the DigitalGlobe imagery, they were compared against the SMA process using root-mean-square error (RMSE), which evaluates the overall estimated accuracy across all samples, and systematic error (SE), which evaluates the effects of systematic errors of overestimation or underestimation (shown below).

(Equation 5 and 6)

$$RMSE = \sqrt{\frac{\sum_{i=1}^{N}(\hat{V}_i - V_i)^2}{N}} \qquad\qquad SE = \frac{\sum_{i=1}^{N}(\hat{V}_i - V_i)}{N}$$

Here $\hat{V}_i$ is the observed (modeled) value produced by the SMA process, while V_i is the 'true' or expected value produced by the visual interpretation of the DigitalGlobe imagery. The reported RMSE and SE were also compared against the error that the SMA process reports (e_b), which represents the amount of variance per pixel that cannot be attributed to any of the endmembers use.

Table 2: Accuracy Assessment

Accuracy Assessment		**Raw SMA (%)**	***Raw SMA Reported % Error***	**Normalized SMA (%)**	***Normalized SMA Reported % Error***	**Raw 4-PC SMA (%)**	***Raw 4-PC SMA Reported % Error***
RMSE	Coban	27.45	*16.35*	15.26	*8.37*	18.68	*25.47*
	İzmit	16.80	*30.56*	16.46	*24.46*	NA	NA
	Semey	15.29	*15.98*	13.13	*16.85*	10.3	*15.73*
SE	Coban	24.23	*16.35*	10.21	*8.37*	14.96	*25.47*
	İzmit	-7.82	*30.56*	-6.70	*24.46*	NA	NA
	Semey	13.10	*15.98*	-6.70	*16.85*	6.90	*15.73*

With regards to RMSE, the results listed in table 2 show that the process of normalizing the bands proposed by Wu (2004) increases the accuracy of the SMA process across all three sites, with the greatest increase in accuracy in Coban, Guatemala, but only slightly for İzmit, Turkey and Semey, Kazakhstan. In addition, the amount of systematic error also decreases using the normalized SMA process for all sites. For SE, both the raw and the normalized SMA process overestimate the amount impervious surface with the exception of İzmit, Turkey, which underestimated the amount of impervious surface in both process. One major change was between the raw SMA and the normalized SMA for Semey which overestimated the amount of impervious surface by 13.10% in the raw SMA but underestimated by -6.7 % in the normalized SMA process. Comparing the SMA reported error (e_b) to the RMSE, it appears that that the SMA process reports an overall error (across all the endmembers) lower than the RMSE of the impervious surface. However, the SMA reported error increased with the normalized SMA process for both İzmit and Semey, while it decreased over Coban.

During the endmember selection for Coban and Semey, an additional SMA process was conducted using raw 4-endmembers per the results of the PC transformation (Coban having vegetation split between bright and dark vegetation and Semey having soil split between bright and dark soil). Comparing the raw 4-endmember SMA against the raw and normalized process showed differences across the sites with Coban producing a large RMSE and SE with a raw 4-endmember SMA compared to a normalized SMA although a significant decrease in both RMSE and SE compared to the raw SMA process. Given that the normalized method is designed to reduce the variance of the endmembers, it is not surprising to a better overall RMSE for the normalized SMA than a raw 4-endmember SMA. However, for Semey, the raw 4-endmember SMA process reduced the RMSE in comparison to both the raw and normalized SMA and decreased the overestimation of the raw process, suggesting that there was difference between the two additional endmembers than the expected variance in brightness (such as what was seen in Coban). Interestingly, the SE of the raw 4-endmember versus the normalized SMA process was virtually the same amount, but opposite with normalized process underestimating the impervious surfaces estimation and the raw 4-endmember SMA overestimating expected impervious surfaces.

Comparing the results of Coban, İzmit and Semey to the reported errors of Columbus by Wu (2004) suggests that the error rate is comparable, yet the results of all three cities were less accurate than the results over Columbus. Wu (2004) reported an overall RMSE of 10.1% and SE of -3.4% for the normalized process with an 18.3% RMSE / -10.8 SE for a 4-endmember SMA and 22% RMSE / 15.9 % SE for the original study conducted by Wu and Murray (2003) (Wu 2004: p 490). In the comparison, Coban appears to show the most variance with regards to SE, being the only site to overestimate the amount of impervious surfaces for the normalized SMA, while both İzmit and Semey both do a better job of underestimating the impervious surfaces than Wu's (2004) Columbus results. Using Wu and Murray (2003) and Wu (2004) as benchmarks—both studies reporting significant increases in accuracy over previous studies done by Ridd (1995), Ward et al. (2000), and Phinn (2002)—the normalized SMA process produce more accurate results with regards to impervious surface estimation.

4.3: Accuracy Assessment: V-I-S model estimation

In addition to the impervious surface accuracy assessment, each AOI was compared as they depicted the urban settings according to Ridd's (1995) V-I-S model. Large sample areas were established by comparing the DigitalGlobe imagery to the component images produced by the SMA process over areas with relatively different urban settings (areas of lower residential density to areas with larger residential density). These sites then had their resulting average V-I-S over the area plotted against Ridd's (1995) model.

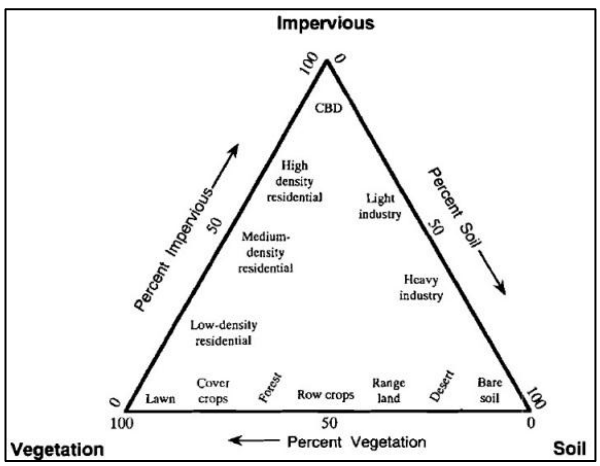

Figure 31: Original V-I-S model from Ridd 1995 p. 2173
The discussion over the screenshots of the V-I-S composition are compared against the original model purposed by Ridd (1995) in figure 31.

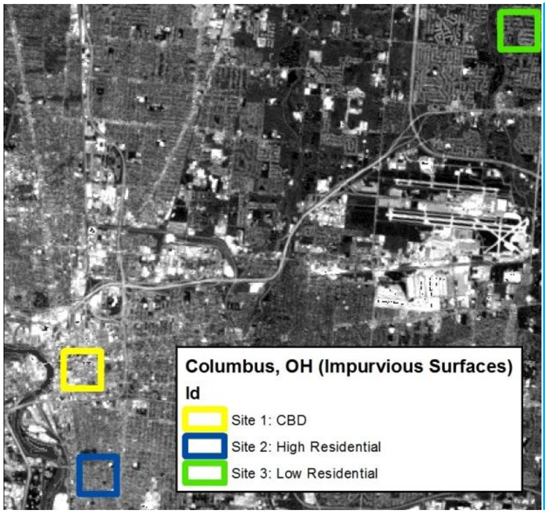

A.

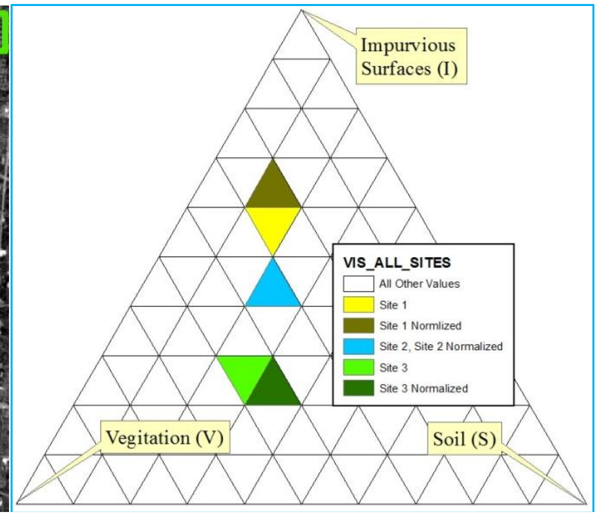

B.

C.

D.

E.

Figure 32: V-I-S Assessment of Columbus, OH. A: Comparative site locations; B: Site V-I-S location on Ridd's model; C: Site 1 CBD; D: Site 2 High Residential; E: Site 3 Low Residential. (C-E show ESRI Imagery Base layer)

Comparing the V-I-S composition of three different sites over Columbus, Ohio, it is easy to identify the relative corresponding location of the different types of urban area. Site 1, the CBD, compared to both site 2 and 3 has a higher percent Impervious Surface ratio and although it has a high percent vegetation than Ridd's (1995) CBD, it is relatively representational compared to the other sites. Site 2 and 3 are representational of the differences along the continuum of higher and lower residential areas, as the ratio of I to S changes. Additionally, the V-I-S composition between the different SMA process indicate that the normalized SMA adjusted the location along the V-I-S model to be more in line with Ridd's (1995) model as well as the results described in Wu and Murray (2003) and Wu (2003).

Coban, Guatemala (seen on Figure 33 on page 65) is a strikingly different urban area compared to Columbus, Ohio. The central part of the city looks to be more like a residential area compared to the large building build up over Columbus, while the residential areas are far less organized and more densely packed. The mixed residential area was labeled as such as there appears to be a large portion of informal settlement compared to the rest of the residential areas. Comparing the V-I-S breakdown over Coban, Guatemala shows a very different representation in comparison to Ridd's (1995) original model. While the CBD is closer to Ridd's (1995) expected CBD ratio compared to the residential areas, it appears to be falling more along the lines of expected light industry. The residential areas, which are very different than the residential areas found in Columbus, Ohio, are described more along the I-S ratio instead of the expected V-S ratio, which Ridd's (1995) model suggest is representational of industry instead of residential

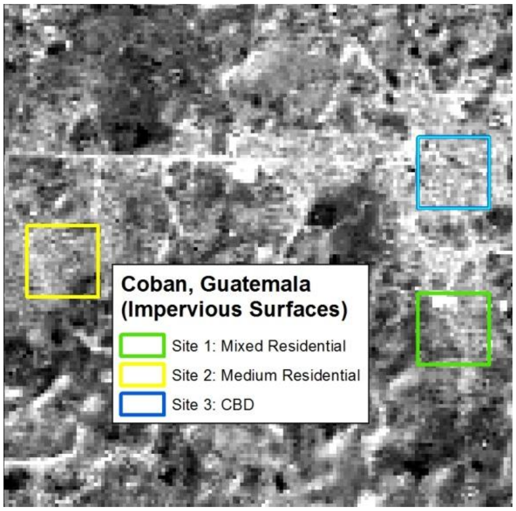

A.

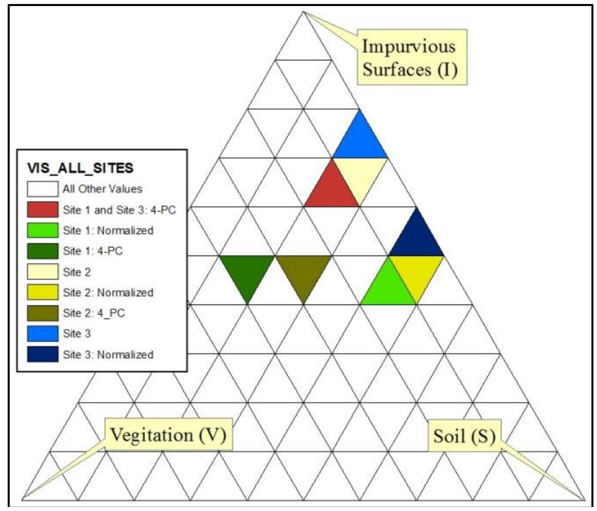

B.

C.

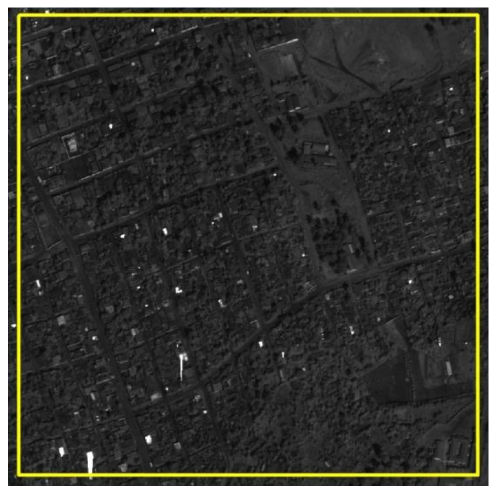

D.

E.

Figure 33: V-I-S Assessment of Coban, Guatemala. A: Comparative site locations; B: Site V-I-S location on Ridd's model; C: Site 1 CBD; D: Site 2 Medium Residential; E: Site 3 Mixed Residential. (C-E show DigitalGlobe imagery)

areas. The normalized SMA changes the ratio, but just slides the two residential sites further Ridd's model from light industry to heavy industry. However, the raw 4-endmember SMA pushes the V-I-S composition closer to the vegetation side, but their composition is nearly identical. It is not possible using Ridd's (1995) model to clearly differentiate between the three sites.

İzmit, Turkey, (seen on Figure 34 on page 67) visually appears to be more similar to Columbus, Ohio with a well developed residential areas surrouded by less developed agricultural areas. At the heart of İzmit are large industrial sites next to the Sea of Marmar. When comparing the first site, which is a large industrial park, to Ridd's (1995) V-I-S model it is not surprising to find it falls within the industrial spectrum. However, the differences (along the V-I-S) model between the industrial site and the high residential site is very slight. According to Ridd's (1995) model what is actually high residential areas is a "heavier industrial" area than the actual industrial area. The third site's composition makes more sense compared to the first two, having more vegetation due to the farmlands and less impervious surfaces to soil ratio, yet is non-descriptive per Ridd's (1995) model as it lies near dead center of the V-I-S continuum. The difference between the raw and normalized SMA process make virtually no difference along the V-I-S model, and in fact pushes all sites closer to the industrial ratio between I-S. While the RMSE and SE for Semey suggested that the raw 4-endmember has the most accuracy at describing the area, it is the most dissimilar to what would be expected from Ridd's (1995) V-I-S model.

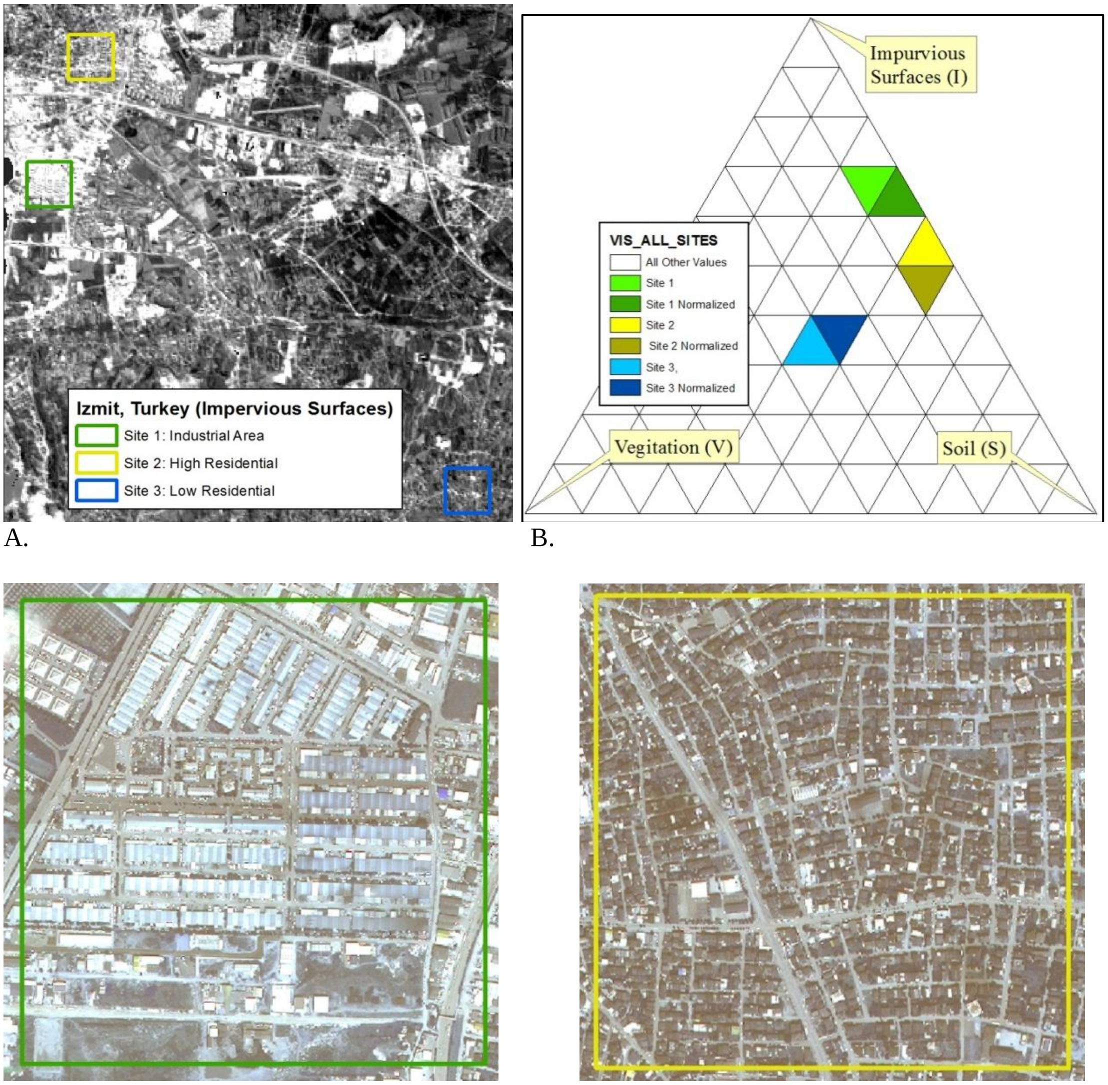

A.

B.

C.

D.

E.

Figure 34: V-I-S Assessment of İzmit, Turkey. A: Comparative site locations; B: Site V-I-S location on Ridd's model; C: Site 1 Industrial; D: Site 2 High Residential; E: Site 3 Low Residential. (C-E show DigitalGlobe imagery)

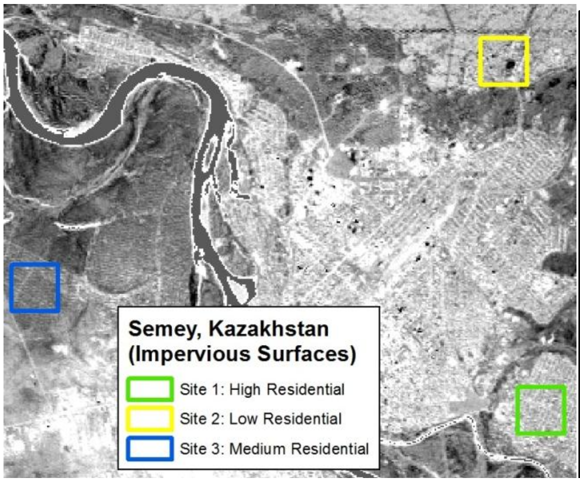

A.

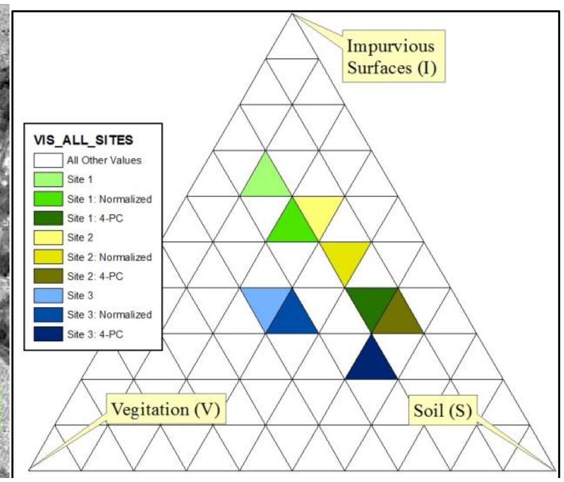

B.


C.

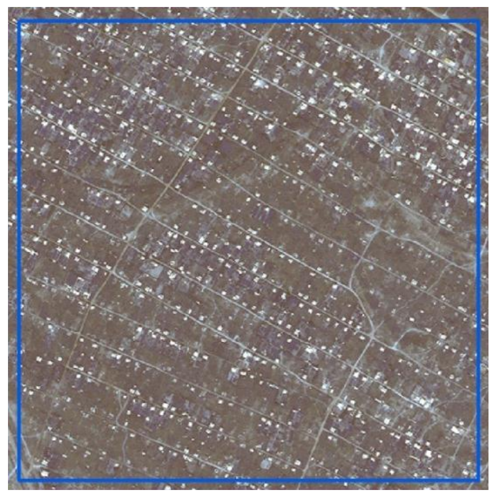
D.


E.

Figure 35: V-I-S Assessment of Semey, Kazakhstan. A: Comparative site locations; B: Site V-I-S location on Ridd’s model; C: Site 1 High Residential; D: Site 3 Medium Residential; E: Site 2 Low Residential. (C-E show DigitalGlobe imagery)

The city of Semey, Kazakhstan, (seen on Figure 35 on page 68) is relatively small compared to Columbus or İzmit in terms of total build up area, but the area is essentially all residential. Additionally, there is much less built up area outside the main area of the city. The three sites used to compare against Ridd's (1995) V-I-S model are all variations along the residential continuum and differ in how densely packed the building are in comparison to open space within the area. With regards to how the three sites fall along the V-I-S continuum of Ridd's urban model, the first site is placed logically compared to the other two sites, with a representationally large percentage of impervious surfaces to vegetation and soil, while sites two and three have less impervious surfaces. Visually, site 2 has more densely packed structures, but per the V-I-S model it is a less residential area than site 3. However, this could also be due in part to the high percent of vegetation making a more distinct difference in the SMA process between % Impervious surfaces and % Vegetation, while in site three there could be a higher rate of error of impervious surfaces due to the higher percentage of soil. The most striking result of the analysis of Semey is the three sites' relative positions along the V-I-S model between the raw, normalized and raw 4-endmember SMA process. In all cases, the normalized SMA and raw 4-endember process moved the sites away from the V-I continuum (residential) and closer to the I-S continuum (industrial) with the raw 4-endmember pushing it the furthest in this direction.

4.3: Summary of Results

In comparison, the results across all four sites paint a very clear picture. While Wu showed that the Normalized SMA process produced more accurate results, both in

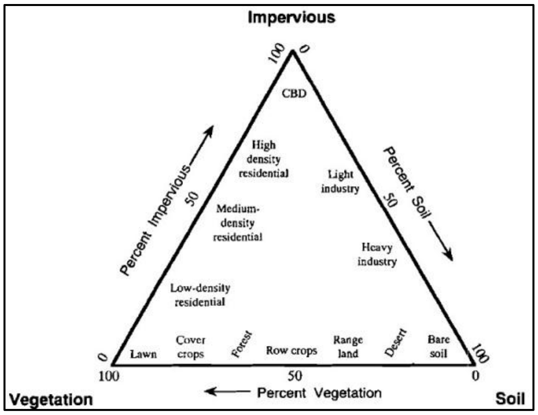

A.

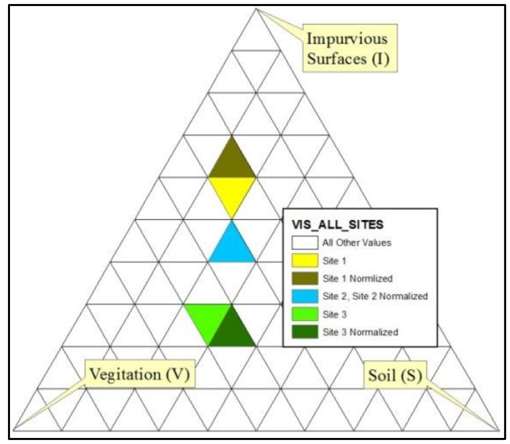

B.

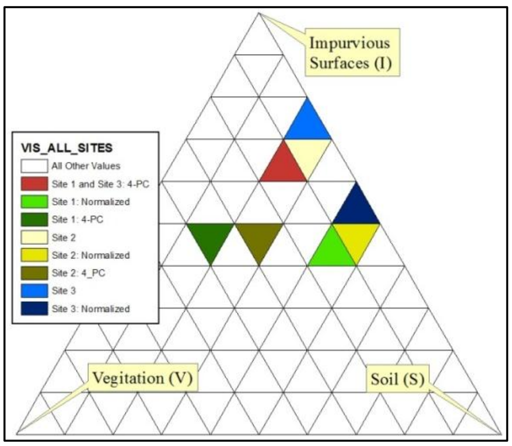

C.

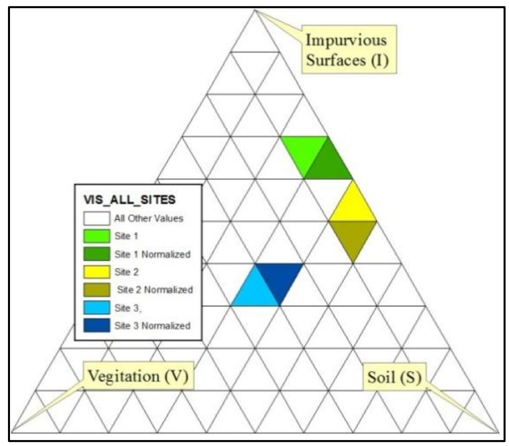

D.

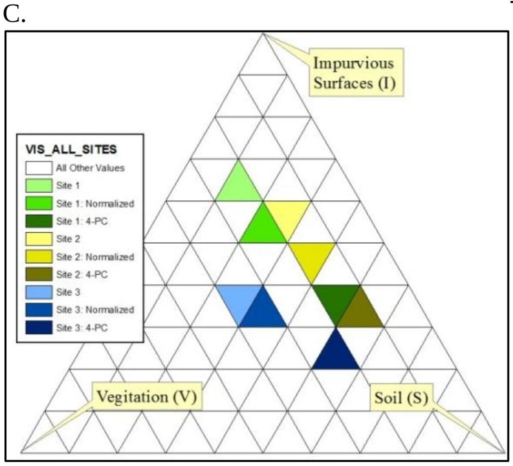

E.

Figure 36: Comparative V-I-S Results.
A: Ridd's V-I-S Model
B: Columbus, OH
C: Coban, Guatemala
D: İzmit, Turkey
E: Semey, Kazakhstan

terms of estimating impervious surfaces and their relationship to Ridd's V-I-S model, Coban, İzmit and Semey indicate that Ridd's model is not indicative of their unique urban composition. Although the tabulated RMSE and SE show that the normalized SMA process is more accurate for estimating impervious surfaces for all locations, the normalized SMA does not provided enough information to balance out the unique characteristic of each site. In particular, the amount of soil in each residential area of Coban, İzmit and Semey dramticaly shift their releitive locations along Ridd's model, which reults in their falling under what Ridd would expect to be inustrialized areas.

CHAPTER 5: CONCLUSION

5.1: First Conclusion

This project has produced two very different conclusions. The first follows the logical argument of how to best define and classify urban setting using remote sensing. With Ridd (1995) we were presented with a methodology to classify urban areas along a continuum of three primary endmembers: Vegetation, Impervious Surface, and Soil. With Ridd (1995) the tools available were low resolution satellite images which were processed using per pixel classification resulting in a less then desired accuracy rate. Following Ridd (1995), many works have discussed methodologies of creating a more accurate process for classifying urban areas, showing a logical move away from per pixel classification to sub pixel classification using spectral mixture analysis (Ward et al. 2000; Phinn et al. 2002; Wu and Murray 2003). With Wu (2004), the classification becomes more precise as errors due to variations in the urban setting are reduced by normalizing the Landsat bands prior to a SMA process. However, all of these works focus primarily on western developed countries. This work shows that using the same procedures developed to extract urban classifications can be applied to areas very different from western areas in terms of material composition. While there are variations in the type of errors produced, the normalized SMA process method provides better results (in particular to impervious surface estimation) across multiple cities. Nevertheless, this work also shows that areas need to be examined for correct endmember classification prior using a normalized SMA. The large variation in bright and dark vegetation in Coban, Guatemala created less error when using a normalized 3-endmember SMA classification than a raw 4-endmember SMA classification, but the opposite was found over Semey, Kazakhstan. In assessing the three sites and comparing them to Columbus, OH, this study argues that using Wu's (2004) normalized SMA process will produce similar results with regards to total error and systematic error.

5.2: Second Conclusion

This project's second conclusion is somewhat at odds with the first conclusion. The primary desire to create a better methodology for extracting the components of an urban setting is offset by the results of how they relate to the original framework of Ridd's (1995) V-I-S model. In the studies reported in this work, Ridd's (1995) V-I-S model was 'proven' to be an accurate method of depicting how remotely sensed data could be explained along an urban continuum, either along the Rural-Urban or Industrial-Urban spectrum (Ward et al. 2000; Phinn et al. 2002; Wu and Murray 2003; Wu 2004). This project does not contradict their findings; in fact the study over Columbus, OH concurs with the reported results by Wu and Murray (2003) and Wu (2004), in that the composition of V-I-S extracted can be used in Ridd's original model to explain the different components of the urban environment. However, this project argues that the effectiveness of Ridd's model is subjective to the location it was derived from. Coban, Guatemala, İzmit, Turkey and Semey, Kazakhstan represent very different urban locations surrounded by very different environments. In all of these cases, Ridd's (1995)

V-I-S model failed to accurately depict, describe or explain the urban classification within the three cities.

5.3: Relationship of the Two Conclusions

In all of these cases, the ratio of soil played a much more significant factor than Ridd's (1995) model would suggest. While the materials classified as impervious surfaces can greatly change from site to site as well as the layout, density or composition of residential building, the accuracy reported in the three sites for representing impervious surfaces was very similar to that Columbus, OH. In addition, the variation of percent impervious surfaces between high and low residential areas was comparable to that of Columbus and Ridd's (1995) model. The major difference in these areas was the relationship between vegetation and soil and their representational relationship to impervious surfaces for depicting residential areas. İzmit and Semey may be outliers, given that the total amount of green vegetation was much lower than Columbus. However, even Coban, Guatemala, which was surrounded by the largest total percent vegetation of all the sites studied, had higher than expected (per Ridd's model) percent of soil in residential areas. More strikingly, when this conclusion is combined with the first conclusion, the normalized SMA process is both more accurate and moves the residential areas of the cities further away from their expected location on Ridd's (1995) V-I-S model.

Without going on-site to these three locations to collect ground truths of the percent vegetation and soil make-up of the residential areas, it is difficult to exactly point to why Ridd's fails to accurately describe the urban areas. One thought is Ridd's (1995) original premise that the definition of ‘vegetation’ is “green vegetation” which has a very distinctive spectral signature, and may move many of other types of vegetation into the exposed earth / soil category. Another thought is that the use of vegetation as a primary endmember to describe residential areas is only applicable to the developed world. While residential areas in developed urban settings such as Columbus, may spend more resources on keeping green vegetation in between other surfaces, or prioritize the utilization of areas to reduce the amount of exposed earth, other less developed areas may not focus their resources or priorities in these similar areas. A third thought is that these cities are located in much more arid environments where the actual % vegetation makes Ridd’s model inappropriate to use. However, this suggestion is again distorted by Coban’s surrounding lush, green vegetation. A final thought is that Ridd’s (1995) model does not accurately separate the classification of residential and industrial areas and that other cities within the developed world would show similar issues as the three sites studied here.

Regardless of the reason why Ridd’s (1995) model does not accurately explain the V-I-S composition of the sites other than Columbus, this study argues that Ridd’s model in its original form is too general to be applicable to every urban setting. While the PC transformation, especially that of the normalize bands, suggest that 3-endmembers can be used to describe these urban settings, this study suggest that a unique continuum of the 3-endmembers would need to be established for each site. In order to do this, a more sophisticated and more complete method of land-use classification would be need to be applied to determine the actual % breakdown of the 3-endmembers and their representation of the urban setting. However, these ‘modified V-I-S (or other A-B-C)’ would be applicable only to their individual sites as opposed to a general model.

5.4: Future Research

With regards to future research, this second conclusion opens many more doors than it closes. While work such as Bhatta et al (2009) have shown the power of using impervious surfaces to explain or describe urban growth and classification using just impervious surfaces, the ability to use a larger endmember spectrum could only help improve the current models. While Bhatt et al. (2009) were able to show urban growth rate, speed and quality (symmetry) of growth, it would be far more telling if the same study could also use the change in vegetation and soil (or other components) in order to better describe the overall change in environments or to place classifications (e.g. CBD, Industrial, low/high residential) on the urban change. In addition, the ability to develop a strong working model similar to Ridd’s (1995) V-I-S is extremely important for studies that want to utilize the large holdings of Landsat data. While 30 meter resolution may be not ideal for urban classification, there is no better continuous data over the entire globe that goes back as far as the Landsat mission. Utilizing techniques such as Wu’s (2004) normalized SMA procedures have proven to increase the accuracy of sub pixel classification. The ability to tie these techniques with more appropriate rural-urban models would dramatically enhance the ability to conduct research outside of developed countries.

Nevertheless, the most important conclusion of this project ties back to the original question: “How does one define an urban area?” While Weeks (2010) and countless other university level textbooks as well as the vast holdings of peer reviewed journals that address this question, this particular project argues that it is extremely difficult to create a one-size-fits-all answer. In reality, a single model generated by the sites listed in this work would encounter difficulties if applied to any number of other areas of the world. Instead, each site needs to be evaluated and have a unique model build for its unique location—both in terms of material composition as well as how the human impact as uniquely shaped the environment. With regards to Week's (2020) chapter on defining urban areas using Ridd's (1995) V-I-S model, or the works by Ward et al. (2000), Phinn et al (2002), Wu and Murray (2003) and Wu (2004) that use Ridd's model, it would be more appropriate to put a stronger disclaimer on the proper use of the model when it is applied to areas outside of where it was originally developed.

BIBLIOGRAHY

Adams, J. B., Smith, M. O., & Gillespie, A. R. (1993). Imaging spectrometry: interpretation based on spectral mixture analysis. In C. M. Pieters, & P. Englert (Eds.), *Remote Geochemical Analysis: Elemental and Mineralogical Composition*, vol. 7 (pp. 145– 166). New York: Cambridge Univ. Press.

Almeida, C. M., Monteiro, A. M. V., Mara, G., Soares-Filho, B. S., Cerqueira, G. C., Pennachin, C. S. L., and Batty, M. (2005). GIS and remote sensing as tools for the simulation of urban land-use change. *International Journal of Remote Sensing*, 26:4, 759–774.

Alparslan, E. Ince, F. Erkan, B. Aydöner, C. Özen, H. Döertas, A. Ergintav, S. Yagsan, F.S. Zaterogullari, A. Eroglu, I. Deger, M. Elasmis, H. Özkan, M. (2008). A GIS model for settlement suitability regarding disaster mitigation, a case study in Bolu Turkey. *Engineering Geology* 26, 126–140.

Aydöner, C. and Maktav, D. (2009). The role of the integration of remote sensing and GIS in land use/land cover analysis after an earthquake, *International Journal of Remote Sensing*, 30: 7, 1697–1717.

Ben-Dor, E., Levin, N., & Saaroni, H. (2001). A spectral-based recognition of the urban environment using the visible and near-infrared spectral region (0.4–1.1 m). A case study over Tel-Aviv. *International Journal of Remote Sensing*, 22(11), 2193– 2218.

Bhatta, B. (2009). Analysis of urban growth pattern using remote sensing and GIS: a case study of Kolkata, India. *International Journal of Remote Sensing.* 30:18, 4773–4746.

Bhatta, B. Saraswati, Bandyopadhyay , S. D. (2009). Quantifying the degree-of-freedom, degree-of-sprawl, and degree-of-goodness of urban growth from remote sensing data. *Applied Geography*, 1–16.

Bonham-Carter, G. (1994). *Geographic information systems for geoscientists: Modeling with GIS*. Ontario: Pergamon. P. 398.

Carlson, T. Arthur, S. (1998). The impact of land use—land cover changes due to urbanization on surface microclimate and hydrology: a satellite perspective. *Global and Planetary Change*, 25, 49–65.

Demirkesen, A. C. (2008). Digital terrain analysis using Landsat-7 ETM+ imagery and SRTM DEM: a case study of Nevsehir province (Cappadocia), Turkey, *International Journal of Remote Sensing*, 29: 14, 4173–4188.

Dubovyk, O. Sliuzas, R. Flacke, J. (2011). Spatio-temporal modeling of informal settlement development in Sancaktepe district, Istanbul, Turkey. *ISPRS Journal of Photogrammetry and Remote Sensing*, 66, 235–246.

Forster, B. C, (1983). Some urban measurements from landsat data. *Photogrammetric Enqineerinq and Remote Sensinq*, 49, 1693-1707.

Gong, P., and Howarth, P. J., (1990). The lise of structural information for improving landcover classification accuracies at the rural-urban fringe. *Photogrammetric Enqineerinq and Remote Sensing*, 56, 67-73.

Green, A. A., Berman, M., Switzer, P., & Craig, M. D. (1988). A transformation for ordering multispectral data in terms of image quality with implications for noise removal. *IEEE Transactions on Geoscience and Remote Sensing*, 26, 65–74.

Irish, R, (1998). Chapter 11: Data product. Landsat 7 science data users handbook, Greenbelt, MD: Goddard Space Flight Center (electronic version, http://landsathandbook.gsfc.nasa.gov/data_prod/prog_sect11_3.html)

Irons, J. R., Weismiller, R. A., & Petersen, G. W. (1989). Soil reflectance. In G. Asrar (Ed.), *Theory and Application of Optical Remote Sensing* (pp. 66– 106). New York, NY: John Wiley and Sons.

Kaya, Ş. , Curran, P. J. and Llewellyn, G.(2005). Post-earthquake building collapse: a comparison of government statistics and estimates derived from SPOT HRVIR data, *International Journal of Remote Sensing*, 26: 13, 2731–2740.

Li, X. & Yeh, A. G. (2003). Analyzing spatial restructuring of land use patterns in fast growing region using remote sensing and GIS. *Landscape and Urban Planning*, 29(2004) 335–354.

Lu, D. & Weng, Q. (2006). Use of impervious surface in urban land-use classification. *Remote Sensing of Environment*, 102, 146–160.

Metternicht, G. I., and Fermont, A., (1998). Estimating erosion surface features by linear mixture modeling. *Remote Sensing of Environment*, 64, 254–265.

Onur, Işin , Maktav, Derya , Sari, Mustafa and Kemal Sönmez, N.(2009). Change detection of land cover and land use using remote sensing and GIS: a case study in Kemer, Turkey, *International Journal of Remote Sensing*, 30: 7, 1749–1757.

Phinn, S., Stanford, M., Scarth, P., Murray, A. T., & Shyy, T. (2002). Monitoring the composition and form of urban environments based on the vegetation-impervious surface-soil (VIS) model by sub-pixel analysis techniques. *International Journal of Remote Sensing*, 23:20, 4131–4153.

Rashed, T., Weeks, J. R., & Gadalla, M. S. (2001). Revealing the anatomy of cities through spectral mixture analysis of multispectral satellite imagery: a case study of the greater Cairo region, Egypt. Geocarto International, 16(4), 5 – 15.

Ridd, M. K., (1995). Exploring a V-I-S (vegetation-impervious surface-soil) model for urban ecosystem analysis through remote sensing: a comparative anatomy for cities. *International Journal of Remote Sensing*, 16: 12, 2165–2185.

Small, C. (2001). Estimation of urban vegetation abundance by spectral mixture analysis. International Journal of Remote Sensing, 22, 1305– 1334.

Small, C. (2002). Multitemporal analysis of urban reflectance. Remote Sensing of Environment, 81, 427– 442.

Sudhira, H. S., Ramachandra, T. V., & Jagadish, K. S. (2003). Urban sprawl: metrics, dynamics and modeling using GIS. *International Journal of Applied Earth Observation and Geoinformation*, 5(2004) 29 –39.

United Nations Population Fund (2007). *State of World Population 2007: Unleashing the potential of Urban Growth*. United Nations Population Fund, New York, NY.

Ward, D., Phinn, S. R., & Murray, A. T. (2000). Monitoring Growth in Rapidly Urbanizing Areas Using Remotely sensed Data. *The Professional Geographer*, 52:3, 371–386.

Weeks, J. R. (2010) Chapter 3: Defining Urban Areas. In T. Rashed and C. Jürgens (Eds.) *Remote Sensing of Urban and Suburban Areas,* Vol. 10 (pp.33–46.) New York, NY: Springer.

Welcii, R., (1982). Spatial resolution requirements for urban studies. *International Journal of Remote Sensing*, 3, 139-146.

Wessman, C. A., Bateson, C. A., and Benning, T. L., (1997). Detecting fire and grazing patterns in tallgrass prairie using spectral mixture analysis. *Ecological Applications*, **7**, 493–511.

Wu, C. & Murray, A. (2003). Estimating impervious surface distribution by spectral mixture analysis. *Remote Sensing of Environment*, 84, 493–505

Wu, C. (2004). Normalized spectral mixture analysis for monitoring urban composition using ETM+ imagery. *Remote Sensing of Environment*, 93, 480–492.

Yates, P. C., (1997). Triangular Coordinates. *Teaching Mathematics and Its Applications*, 16:1, 23–26.

Yonezawa, C. (2007). Maximum likelihood classification combined with spectral angle mapper algorithm for high resolution satellite imagery. *International Journal of Remote Sensing*, 28: 16 3729–3737.

Yuan, F., and Bauer, M. (2007). Comparison of impervious surface area and normalized difference vegetation index as indicators of surface urban heat island effects in Landsat imagery. *Remote Sensing of Environment*, 106, 375–386

CURRICULUM VITAE

Caleb E. Gaw graduated from Colorado Rocky Mountain School, Carbondale, CO in 2000. He received his Bachelor of Science from the United States Air Force Academy in 2004. He is currently employed at Science Application International Corporation as a GIS analysis and is working on his Master of Science in Geoinformatics and Geospatial Intelligence from George Mason University.